The Thesis Committee for Edna Rodriguez Calzado

Certifies that this is the approved version of the following Thesis:

Estimating CO_2 Storage Capacity, Injectivity, and Storage Costs for Large-Scale CCS Deployment & Carbon Dioxide Removal Goals

APPROVED BY

SUPERVISING COMMITTEE:

Susan D. Hovorka, Co-Supervisor

Alexander P. Bump, Co-Supervisor

Ramón H. Treviño, Reader

Estimating CO_2 Storage Capacity, Injectivity, and Storage Costs for Large-Scale CCS Deployment & Carbon Dioxide Removal Goals

by

Edna Rodriguez Calzado

Thesis

Presented to the Faculty of the Graduate School of

The University of Texas at Austin

in Partial Fulfillment

of the Requirements

for the Degree of

Master of Science in Energy and Earth Resources

The University of Texas at Austin

May 2023

Dedication

This thesis is dedicated to my late grandmother, María de los Ángeles Vázquez, whose tenacity and strong spirit made me into the person I am today.

Acknowledgements

I would like to start by thanking both of my supervisors, Dr. Susan D. Hovorka and Dr. Alexander P. Bump, for their immense support, contributions, and guidance throughout my academic journey. Both of their expertise in CCS is immeasurable, and I am truly fortunate to have had them both as my supervisors.

I would also like to thank the Gulf Coast Carbon Center (GCCC) for both their academic and financial support throughout the past couple years. This work is part of the Roads to Removal: US Department of Energy by the Lawrence Livermore National Laboratory (contract DE-AC52-07NA27344), as well as the Southeast Regional CO_2 Utilization and Storage Acceleration Partnership – SECARB USA, U.S. Department of Energy/NETL DE-FE0031830. To Ramon Treviño, my thesis reader, for always being so welcoming. Thank you to all the other researchers at the GCCC for their support.

I am also thankful for the support of the Energy and Earth Resources (EER) program and fellow EER classmates. The professional fund provided by the EER allowed me to travel and present part of my thesis work at a renown national conference. To my fellow EER classmates and BEG girlies, Angela, Yushan, and Katherine for their enriching friendship throughout the process. I am grateful that I got to work alongside such a talented, diverse, and passionate group of individuals. Thank you for accompanying me on walks to the Starbucks on Burnet and Braker Lane to destress from the thesis/academic work.

Lastly, I would like to thank my mother, Edna Maria, for her unwavering support in what I am passionate about throughout not just these past couple of years, but throughout my life. You deserve the world, mom.

Disclaimer: "This report was prepared (in part if that is relevant) as an account of work sponsored by an agency of the United States Government. Neither the United States Government nor any agency thereof, nor any of their employees, makes any warranty, express or implied, or assumes any legal liability or responsibility for the accuracy, completeness, or usefulness of any information, apparatus, product, or process disclosed, or represents that its use would not infringe privately owned rights. Reference herein to any specific commercial product, process, or service by trade name, trademark, manufacturer, or otherwise does not necessarily constitute or imply its endorsement, recommendation, or favoring by the United States Government or any agency thereof. The views and opinions of authors expressed herein do not necessarily state or reflect those of the United States Government or any agency thereof."

Abstract

Estimating CO_2 Storage Capacity, Injectivity, and Storage Costs for Large-Scale CCS Deployment & Carbon Dioxide Removal Goals

Edna Rodriguez Calzado, M.S. E.E.R.

The University of Texas at Austin, 2023

Supervisors: Susan D. Hovorka, Alexander P. Bump

Large-scale deployment (i.e.,, nationwide) of Carbon Capture and Storage (CCS) technology will play a key role in carbon storage removal (CDR) and overall climate mitigation efforts. The economic feasibility of large-scale CCS deployments partly depends on the CO_2 storage costs per project. However, the suitability of regional storage and injectivity per project, particularly for large-scale purposes, is not well understood.

This study focuses on two concepts that augments existing studies of storage capacity and cost to assess the opportunities and barriers to CDR. The first concept focuses on identifying all potential areas for CO_2 storage within the sedimentary rocks throughout the U.S. based on a novel concept we call the CO_2 Storage Window. The second concept focuses on improving CO_2 storage costs estimates by considering 1) the number of wells needed to inject at a certain rate, dependent on injectivity of the area and 2) the areal extent of pressure build-up caused by CO_2 injection. This area extent is a novel concept we call pressure space. Understanding the pressure space of a project helps delineate the area of review for a project and the extent of the pore space required for the project.

The results of this study include a spatial geodatabase and a series of U.S. cohesive, spatial distribution maps showcasing 1) CO_2 storage potential in areas not explored before, 2) Storage costs per CCS project and storage costs per ton of CO_2, assuming a constant maximum storage capacity of 20 Mt per project over a 20-year timeframe, and 3) Estimated storage costs per ton of CO_2 in areas where storage potential is found but where there is not enough data to calculate capacity nor injectivity.

Table of Contents

Acronyms

CCS	Carbon Capture and Storage
CO_2	Carbon dioxide
CDR	Carbon dioxide removal
DAC	Direct air capture
GCCC	Gulf Coast Carbon Center
GHG	Greenhouse gas
Gtpa	Gigatons per annum
Mtpa	Million tons per annum
USDW	Underground source of drinking water
USGS	United States Geological Survey

List of Tables

List of Figures

Chapter 1: Introduction

1.1 BACKGROUND

The need and dramatic implementation of climate change mitigation techniques, such as Carbon Capture and Storage (CCS), is more important than ever. According to the 2014 IPCC's Mitigation Against Climate Change report, CCS technology is critical to reach the greenhouse gas emissions' (GHG) reduction goal of keeping global temperatures from rising over the 2°C baseline and limiting the detrimental impact of carbon dioxide (CO_2) emissions on the world (IPCC, 2014). CCS technology and science aims to remove CO_2 from either the atmosphere or from the source and store it in the subsurface permanently to reduce CO_2 concentrations in the atmosphere. To meet the GHG goal, the Biden Administration established a net zero GHG goal by the year 2050, which will be assisted by a 1 Gigaton per annum (Gtpa) of carbon dioxide removal (CDR) goal from the atmosphere into the subsurface (U.S. Dept. of State, 2021).

In order to reach the Biden Administration's net zero goal, the U.S. needs to deploy and upscale the development of CCS projects as quickly as possible. As of 2022, there are a total of 35 CCS projects collectively storing 45 million metric tons per annum (Mtpa) globally, with around 300 new projects in development set for completion by 2030 (IEA, 2022b). In the U.S., there are 19 operational CCS facilities (of which 12 are commercial and seven are demonstrations projects) storing around 25 Mtpa, with 22 CCS facilities in development (Figure 1.1). However, a recent study determined that the current and planned CCS projects will not be enough to meet the net zero goals set by the Biden Administration (Figure 1.2).

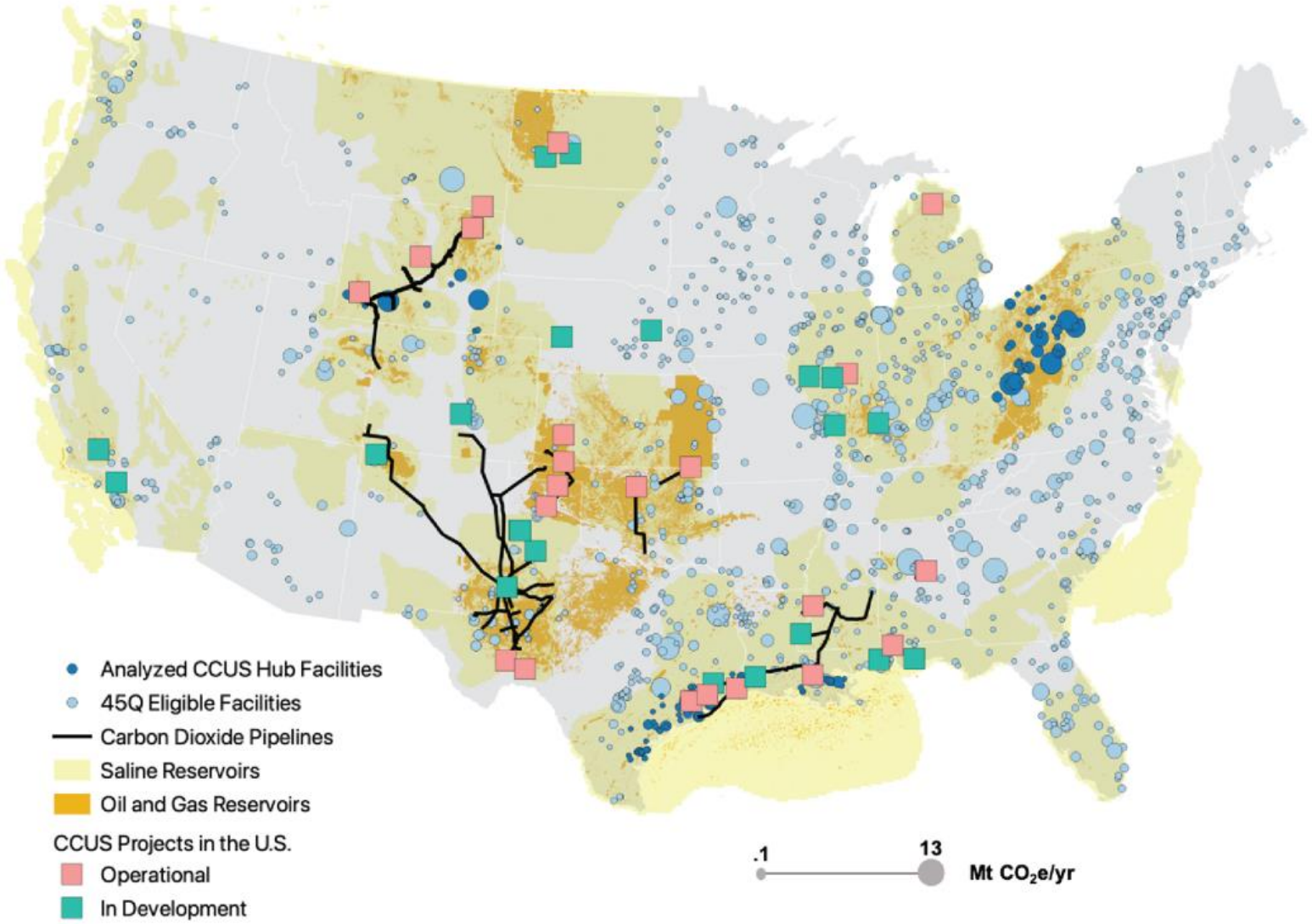

Figure 1.1 : Major CO2-Emitting Facilities, CCUS Projects, and CO2 Pipelines in the United States (Taken from the Labor Energy Partnership report, 2021).

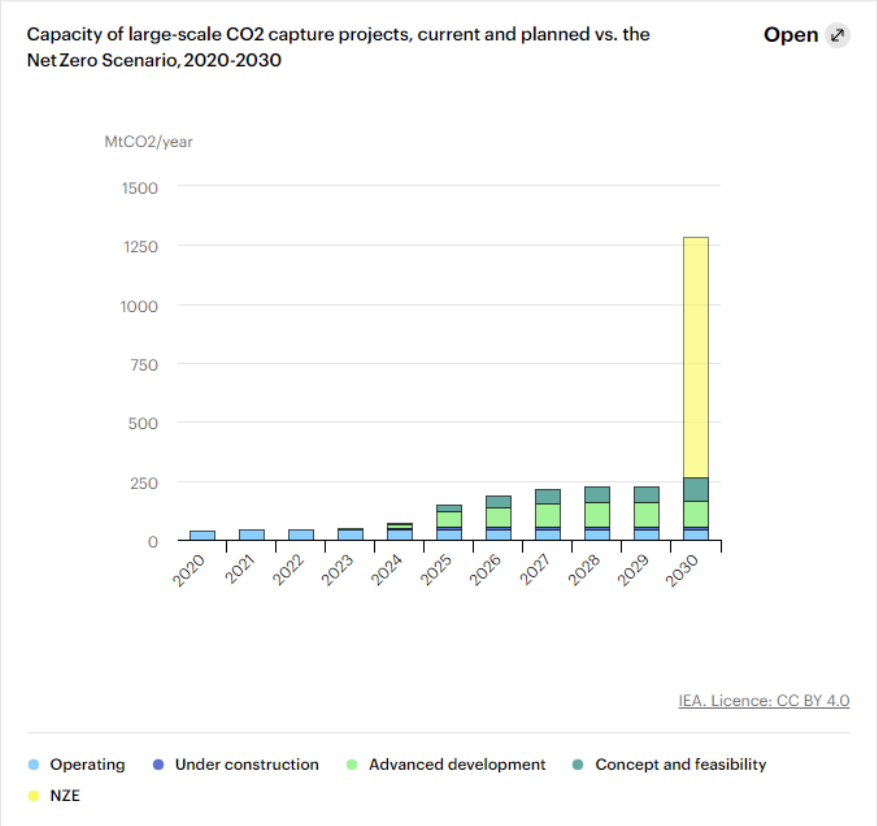

Figure 1.2: Capacity of large-scale CO2 capture, current and planned vs. the Net Zero Scenario, 2020-2030 (IEA, 2022a).

Reaching the CDR goal of 1 Gtpa depends on the scalability of CCS, but more importantly, it depends on the availability and suitability of storage to match the demand from carbon capture technologies. A recent report by the Lawrence Livermore National Lab indicated that the U.S. has the ability to meet the CDR goal and even go beyond removing over 1 Gtpa (Pett-Ridge, 2022). The capture technologies involved in this assessment are direct air capture (DAC) and biomass carbon removal and storage (BiCRS). DAC and BiCRS will rely on permanent storage, like CCS, to meet their CDR goal quotas.

However, the availability and suitability of storage in large-scale CCS deployment and CDR goals is not well understood. For instance:

1. Is there enough storage capacity/injectivity to meet local demand where DAC or BiCRS technology are deployed?
2. Is the capacity sufficient for large point source facilities using CCS to reduce emissions from fossil fuel combustion, ethanol, or cement manufacture where they exist?
3. If we are to upscale CCS for net zero and CDR goals, how do we manage neighboring CCS projects and mitigate risks of overpressure?
4. What about areas where there has been no storage capacity nor injectivity study? Is there potential for storage in areas we do not know about?
5. How much is CCS going to cost? What exactly goes into determining cost?

One way to address the suitability of storage at a given location is by providing development cost estimates that consider the geologic reservoir's properties. A CCS project's development costs include the capture, transportation, and storage of CO_2. It is common practice for investors to require the development costs and financial impact of a project before investing in or developing a CCS project. If a project's financial impact does not produce a profit, it is likely that the project will not be developed. However, to accurately estimate development costs, specifically storage costs, a general understanding of the geologic properties and their limitations should be considered. For example, the storage capacity (i.e., how much CO_2 can be stored) depends on a rock unit's physical properties, such as permeability and porosity. These properties change depending on the type of rock available in the subsurface. Since injectable zones in the subsurface vary in

size, shape laterally and horizontally across an area, calculating storage costs is not straightforward and is generally a challenging task.

1.2 PREVIOUS WORK

There are several storage costs models available publicly today; the most commonly utilized is the SimCCS software developed by Carbon Solutions LLC (Middleton et al. 2020b). SimCCS is a software simulation tool developed over the past decade to optimize CCS infrastructure decisions. The tool encapsulates CO_2 capture, storage, and transportation costs, as well as the associated infrastructure and regulation costs. Other cost tools have been developed, such as the NETL CO_2 Saline Storage Cost model (NETL, 2017). However, the multivariate optimization, flexible modeling, and optimized cost methodology calculation capabilities of SimCCS outperform these other tools (i.e., SimCCS vs NETL storage costs, Ogland-Hand et al. 2022). Consequently, multiple CCS infrastructure and energy optimization frameworks in other studies have utilized the SimCCS software to calculate costs (Middleton et al. 2020b).

Carbon Solutions LLC developed software packages for storage, capture and transportation costs, including the SCO_2T^{PRO} package specifically for storage costs. This package is capable of providing dynamic CO_2 storage capacity, injection rates, and plume radial extent results by inputting geological parameters (i.e.,, depth, porosity, permeability, etc.) into a reduced-order model simulation (Middleton et al 2020a). Additionally, the package can calculate storage costs based on the output capacity and injectivity results and the EPA GCS cost model (EPA, 2010).

With their SCO_2T^{PRO} package, Carbon Solutions LLC produced the newest nationwide estimates of realistic CO_2 storage costs. Figure 1.3 showcases the geospatial distribution of the resulting SCO_2T^{PRO} storage costs. Although the source of Figure 1.3

does not specify the data inputs utilized to calculate the storage costs displayed, it is possible that the NETL's NATCARB national database, as well as the U.S. Geological Survey's carbon dioxide storage assessment database were utilized to achieve such a task (Bennet et al. 2022).

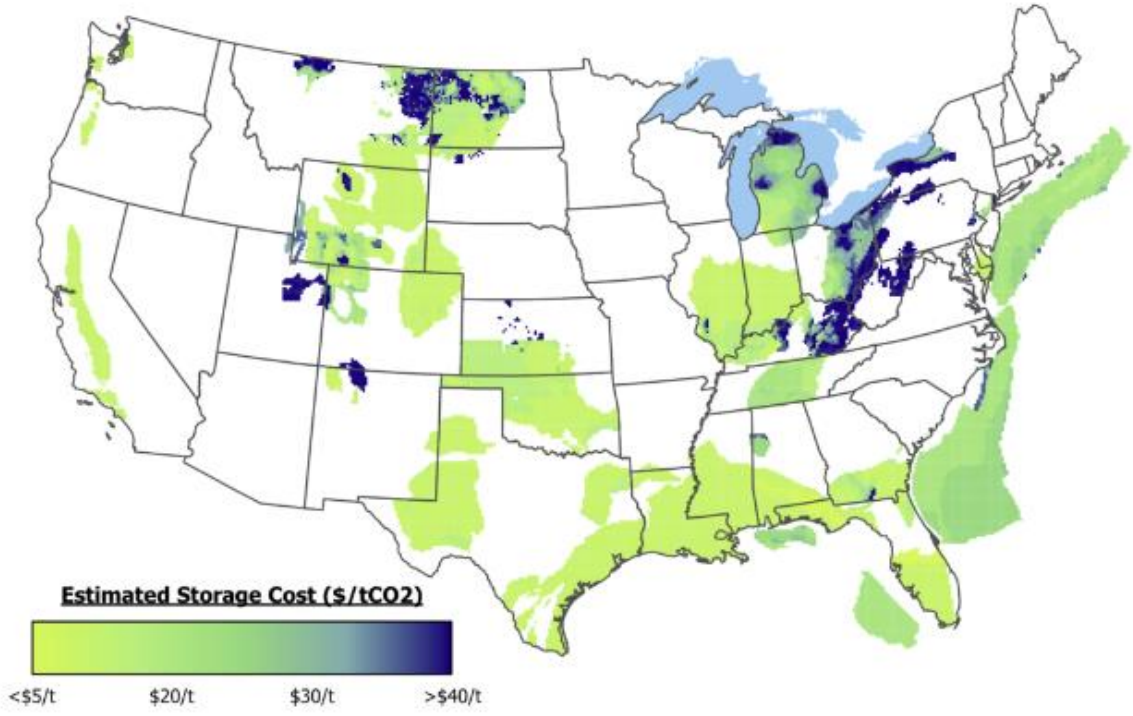

Figure 1.3: SCO_2T^{PRO} estimated storage costs ($/ton of CO_2) (Carbon Solutions LLC, 2022).

Although SimCCS provides nationwide storage cost estimates, they still do not fully provide a storage cost picture at a national scale. For example, what is the cost of storage in states like Nevada and Arizona, where the Basin and Range physiographic region exists and there are known sedimentary rock units that could be potentially useful for CO_2 storage. Furthermore, there are other national input datasets they have not considered for

this storage cost assessment, such as the Gulf Coast Carbon Center's brine database (GCCC, 2013).

1.3 PROJECT GOALS

Large-scale deployment of CCS in an optimized, rapid, cost-effective manner requires understanding the availability and suitability of storage, including issues relevant for obtaining CDR goals. Consequently, the main goals of this thesis are to:

1. Explore and identify areas where potential CO_2 storage is physically possible, and equally as important, where it is not.

   This is achieved by re-evaluating storage feasibility in sedimentary rocks using national spatial data. Several storage criteria are used to limit what is and what is not considered storage potential within a given physical window. As a result, the storage window concept is created, and is displayed as a cohesive, U.S.-wide map.

2. Understand the suitability of CCS in a given area by providing new CO_2 storage costs based on a new cost methodology that considers optimized regional storage capacity and injectivity calculations.

   The new cost methodology is based on the number of wells and area per project. The number of wells is derived from injectivity calculations, while the area per project is derived from storage capacity. Both injectivity and capacity are optimized by incorporating greater spatial resolution geologic data. Capacity is further optimized by considering pressure-based area limitations. Storage costs are also

estimated for areas within the storage window that do not have geologic data to calculate capacity or injectivity. Capacity calculations in this thesis are a combination of volumetric and performance-based estimates as defined by the storage resources management system (Frailey et al. 2017).

3. Provide maps and prepare a spatial database for public use.

The "CO_2 Capacity, Injectivity, and Cost" database is included as supplementary data to this thesis. This database contains three main spatial datasets: 1) "*Capacity Injectivity Cost Data",* 2) "*Highest Injectivity Analysis*", and 3) "*CO_2 Sedimentary Storage Window*". The datasets are saved within an ArcGIS geodatabase (.gdb) as feature classes and can only be accessed using the ArcGIS software. Further details on data acquisition, processing, and structure are found in Chapter 6.

Chapter 2: Sedimentary CO_2 Storage Window

2.1 INTRODUCTION

Although the idea of a CO_2 storage capacity interval has been around for a while (Wallace et al. 2014), sedimentary CO_2 storage window is a term coined recently within the CCS community (Bump et al 2021). The sedimentary CO_2 storage window (SSW) is the depth range in a sedimentary geologic section where CO_2 can be conventionally stored in a dense or supercritical phase in permeable porous rocks and below fracture pressures. Sedimentary rocks are the target of conventional CO_2 storage in that they allow for the injection and containment of CO_2, as the rocks tend to have suitable porosity and permeability. More importantly, sedimentary rocks tend to contain alternating layers of porous/permeable material, like sandstone, and non-porous/non-permeable material, like shale, that create a natural trapping mechanism for the injected CO_2 underground and prevents unwanted CO_2 upward migration. Other rock types such as shales, coals, chemically reactive mafic and ultramafic rocs have been considered for storage (NETL, 2015), however the storage processes and maturity are different enough that these options are not included in the scope of this study.

This study provides a new national-scale dataset of a sedimentary CO_2 storage window across the U.S. The SSW dataset can help achieve the following goals:

1. To accelerate carbon dioxide removal (CDR) goals, identify marginal and/or unexplored potential storage areas where SSW exists.
2. Improve formation-wide pressure space and injectivity spatial data calculations by limiting calculation results to within the SSW (refer to section 3.3.1).

2.2 CALCULATING THE SEDIMENTARY CO2 STORAGE WINDOW

The sedimentary CO_2 Storage Window (SSW) is calculated by taking the difference between the depth to the bottom storage window boundary and the depth to the top storage window boundary (eq. 2.1). A positive SSW result signifies that the area does have the potential for storage, while a negative SSW result means no storage potential in that area.

$$SSW = depth\ to\ bottom\ boundary - depth\ to\ top\ boundary \quad (2.1)$$

The top and bottom CO_2 storage window boundaries delineate physical boundaries in sedimentary formations within which CO_2 can be stored conventionally (Figure 2.1). The shallowest depth at which CO_2 remains in a supercritical state defines the top window of SSW. CO_2 in a supercritical state allows for a higher volume of CO_2 to be stored within a given volume of porous rock. The top SSW depth is estimated with a simplification to be 750 meters below the top of groundwater. The bottom window delineates the base of the sedimentary rock below which Precambrian-aged basement rocks begin. The Gulf of Mexico Basin formations are an exception in that the bottom window represents depth to top of overpressure rather than base of the sedimentary rock section.

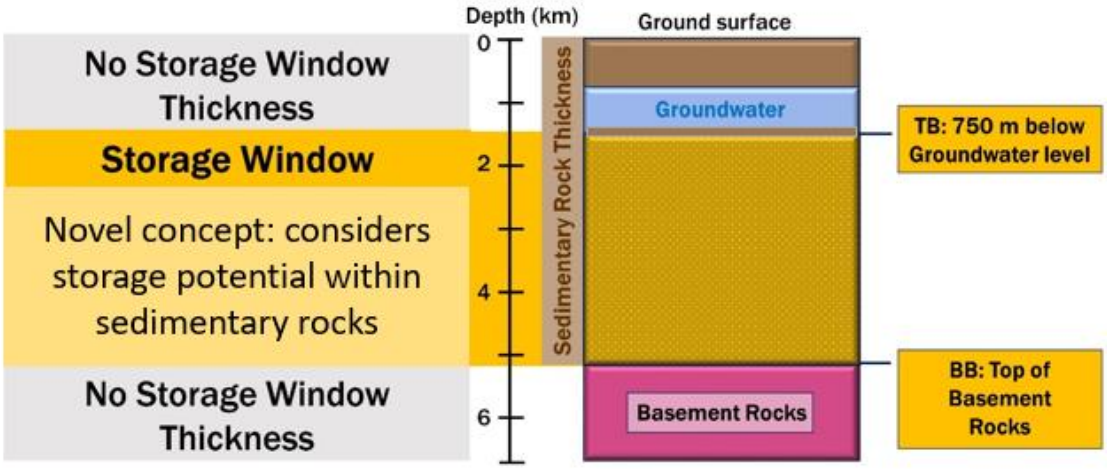

Figure 2.1: Sedimentary CO2 Storage Window (SSW) Schematic. TB = Top SSW Boundary, BB = Bottom SSW Boundary.

2.3 SEDIMENTARY CO2 STORAGE WINDOW INPUT DATA

Calculation of the Storage Window is the result of the compilation, editing, and grid algebra applied to preexisting spatial data. To process and edit the data, ArcGIS software and tools (i.e.,, Raster Calculator) were utilized for spatial data calculations. Table 2.1 below summarizes the input data and data sources utilized to calculate both the top and bottom SSW boundaries.

Storage Window Analysis	Input Data	Section	Data Sources
Top SSW boundary	Depth to Groundwater Table	2.3.2	De Graaf et al. 2017
	Continental Digital Elevation Models	2.3.3	Porter et al. 2018
			USGS 3DEP 2022
Bottom SSW boundary	US Wide Sedimentary Rock Thickness	2.3.1	Laske and Masters 1997
			Marshak et al. 2017
			Shah et al. 2018
	Depth to Overpressure (GOM only)	2.3.4	Burke et al. 2012

Table 2.1: Storage Window Analysis input data summary table.

2.3.1 U.S-WIDE SEDIMENTARY ROCK THICKNESS

Three sources delineating different regions in the U.S. (western U.S. (Shah et al. 2018), central U.S. (Marshak et al. 2017), and eastern U.S. (Laske and Masters, 1997)) were utilized and modified to create a cohesive, national-scale sedimentary rock thickness dataset. To merge all three sources, contour lines were created from each data source, and later rasterized utilizing ArcGIS's topo to raster interpolation tool. The western U.S. sediment thickness map covers the western states and continues on east until reaching the Precambrian basement craton edge (Shah et al. 2018). Unlike the central and eastern U.S. sources, where sedimentary thickness extends to the Precambrian basement, the western

U.S. thickness map includes sediment thickness up to the top of Mesozoic basement. Additionally, the contour lines in the eastern U.S. data source were edited such that they did not overlap with data from the central U.S. data source in order to avoid overlapping sources of data when compiling all three data sources together.

2.3.2 DEPTH TO GROUNDWATER

The groundwater depth data utilized for this project is a two-layer global groundwater model utilizing a combination of the hydrological model PCR-GLOBWV and a groundwater model using MODFLOW (De Graaf et al 2017). The model is presented in monthly time-steps with December 2015 as the last iteration of the model. Thus, December 2015 was chosen to represent the depth to top of groundwater. The global groundwater model is split into two layers, Layer 1 and Layer 2. Layer 2 is described as the top of the confining geological layer, while Layer 1 is the top of the confined aquifer underneath it. De Graaf et al. (2017) delineated the layers based on grain sizes of unconsolidated sediments (GLiM). Since De Graaf et al. defines Layer 1 to include top of "partially" confined aquifers as well (meaning there is still transmissivity through Layer 1 to Layer 2), this study utilizes Layer 2 to represent depth to top of groundwater.

2.3.3 CONTINENTAL DIGITAL ELEVATION MODELS (DEM)

Continental Digital Elevation Models from the lower 48 states (USGS 3DEP, 2022) and Alaska (Porter et al. 2018) were utilized to edit spatial datasets. For example, the central US original database (Marshak et al. 2017) provided depth to top of Precambrian basement relative to mean sea level, so therefore 3DEP DEM data were needed to create an accurate sediment thickness map of this data source. DEM data were also utilized to exclude areas of steep elevation change, as further explored in section 2.4.2.

2.3.4 DEPTH TO OVERPRESSURE

Burke et al. (2012) is comprised of a geopressure-gradient model consisting of 200,000 mud-weight measurements from 70,000 wells which resulted in depth contour maps of these geopressure-gradient surfaces ranging from 0.6 psi/ft to 1.0 psi/ft in the Gulf of Mexico Basin. This thesis utilizes the geopressure-gradient surface of 0.7 psi/ft to delineate depth to top of overpressure in the Gulf of Mexico Basin, as this surface is considered to represent the top of the overpressure transition zone (Harrison, 1980).

2.4 NO STORAGE WINDOW CRITERIA

This section discusses the three no storage window criteria considered for the SSW data. All three compose the no storage window spatial data that complements the SSW data.

2.4.1 INSUFFICIENT SEDIMENTARY THICKNESS

In some areas of the U.S., particularly in the western states, there is a lack of sufficient sedimentary thickness to successfully store CO_2 in the subsurface. As previously mentioned, CO_2 needs to be stored deeper than 750 meters below groundwater level to maintain its supercritical fluid state. If there is less than 750 meters of sediment thickness, then the top window is deeper than the total extent, and thus no conventional supercritical storage potential is available in this location.

2.4.2 GEOLOGIC AND TOPOGRAPHIC CONSTRAINTS

When considering the extent of potential CO_2 storage, it is important to consider the constraining impact of different types of rock on storage. For example, there are types of rocks that do not have matrix porosity and permeability, only fracture permeability. Such rocks include Precambrian rocks (conterminous U.S.: Schruben et al 1997, Alaska: Wilson

et al 2015), metamorphic rocks, and glaciers (Garrity and Soller, 2009). The areas where these types of rock exist have been excluded from potential CO_2 storage consideration. Storage in igneous rock is excluded from the scope of this work, and thus has been included in the geologic constraint criteria.

When considering the extent of potential CO_2 storage, it is also necessary to exclude areas of steep elevation (i.e.,, mountain ranges) where storage infrastructure construction and logistics are complicated. For the conterminous U.S., this work has only highlighted the Appalachian and Ouachita Mountain ranges (spatial data taken from Marshak et al. 2017). For Alaska, DEM data (Porter et al. 2018) was utilized to filter out any areas with an elevation higher than 1000 meters. The results of this DEM filter show the extent of all three main mountain ranges in Alaska.

Chapter 3: Pressure-Based CO_2 Storage Capacity Methodology

3.1 INTRODUCTION

In recent years, there has been a shift from volumetric capacity estimates to pressure-based capacity estimates. This is due to the understanding that pressure build-up from CO_2 injection is a key limiting factor for capacity estimates and is more relevant to project costs than the saturation of the injected CO_2 plume used in previous work. If the pressure increase is not properly managed, the subsurface can become overpressured and cause unwanted consequences, such as fracturing of the injection zone or confining system and would exceed the specifications of Class VI permits. This issue becomes more pressing for large-scale CCS deployment, elevating importance for this work looking at large-scale injection.

This study focused on optimizing regional storage capacity estimates using a new concept defined as pressure space (Bump and Hovorka, personal communication), which delineates the area extent caused by pressure increase from CO_2 injection, and more importantly, the maximum areal extent of a CCS project. Dr. Bump's pressure space concept builds upon the work done by Mathias et al. (2009) and Van der Meer and Yavuz (2009) on the screening and selection of CCS project sites based on pressure buildup. As CO_2 is injected into the subsurface, the resulting pressure increase extends outward from the injection well, surpassing the plume itself (Figure 3.1). Since the extent of the pressure increase is the maximum amount of area affected by CO_2 injection within a CCS project, it can be considered as the total area of a CCS project.

More importantly, establishing the pressure space needed to support a project directly relates to the total storage costs related to a project. The costs of 2D and 3D seismic exploration of the project site, monitoring, and acreage of pore space lease all depend on

the extent of the project itself. As an example, high resolution 2D seismic on flat terrain can cost up to $25,000 per mile (NETL, 2013).

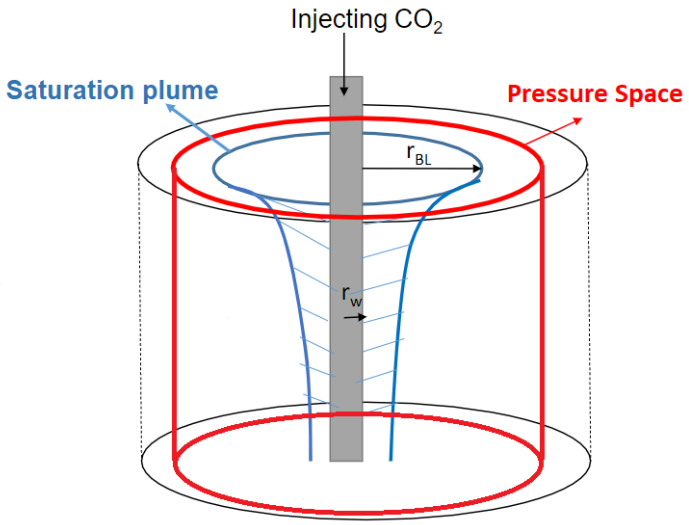

Figure 3.1: CO_2 saturation plume and pressure build-up (Pressure Space) propagation in the subsurface (modified from S. Bakhshian, unpublished figure).

Additionally, pressure space is a key concept that can clarify overlapping interests, such as subsurface pore space property rights, from parties involved in the large-scale deployment of CCS, which include investors, regulators, and landowners. Rules and regulations in the U.S. as to who owns the pore space within a geologic reservoir are administered by states (Ivory-Moore, 2022). In many states, pore space ownership is allocated to the land surface owner. However, pore space is not limited by surface boundaries (e.g., state or national boundaries); consequently, it is likely that multiple landowners could be involved in a single CCS project. Some argue that ownership should be vested to the public to hasten CCS deployment (Zadick, 2011), but regardless of who

owns the pore space, if there is no clear delineation of the legal property involved, a large-scale deployment of CCS is not possible (Fish and Wood, 2008). Therefore, pressure space and delineating the total area of a project come into play - if the area per project can be established, then pore space ownership discussions between regulators, landowners, and investors can be clarified and solved.

3.2 CALCULATING PRESSURE-BASED CO2 STORAGE CAPACITY

Pressure space considers the induced pressure increase and propagation from injected CO_2 within a porous volume in a given geologic formation (eq. 3.1):

$$\text{Pressure Space} = (\text{Allowable Pressure Increase}) * (\text{Pore Volume}) \quad (3.1)$$

Pressure-based CO_2 storage capacity takes the concepts of pressure space as given in equation 3.1, and can be rewritten with the following parameters:

$$Cap_P = \frac{(P_I * C_T * \rho_{CO2}) * (\Phi * A * SWFT * N{:}G)}{1000} \quad (3.2)$$

Where the parameters are:

Cap_P is Pressure-based Capacity (in million tons (Mt) of CO_2)
P_I is Pressure Increase (MPa)
C_T is Total Compressibility (1/MPa)
ρ_{CO2} is CO_2 Density (kg/m^3)
Φ is Porosity (decimal)
A is Area (m^2)
SWFT is Storage Window Formation Thickness (m)
$N{:}G$ is Net to Gross injectable interval (decimal)

3.3 PRESSURE-BASED CO_2 STORAGE CAPACITY PARAMETERS

The parameters considered to calculate pressure-based CO_2 storage capacity are a combination of 1) input data from sources like the Gulf Coast Carbon Center's (GCCC) CO_2 Brine database (GCCC, 2012) and U.S. Geological Survey's Carbon Dioxide Storage Assessment (USGS, 2013), 2) calculated parameters from input data (i.e.,, Midpoint Formation Depth, MDF), and 3) calculated parameters derived from other calculated

parameters (i.e., CO_2 density). The acquisition of supplementary input data and processing will be further discussed in Chapter 6.

3.3.1 STORAGE WINDOW FORMATION THICKNESS

The Storage Window Formation Thickness (SWFT, meters) is the total thickness of a given reservoir formation within the sedimentary CO_2 Storage Window (SSW). The goal is to omit any part of the geologic section that would not be feasible to store CO_2 long-term.

The USGS database (USGS, 2013) provides storage window formation thickness data, but two steps are required to calculate SWFT for the GCCC database:

1. Delineate the Storage Window Area (SWA, meters squared): The SWA is the 2D spatial extent calculated from subtracting the depth to top window boundary (refer to section 2.2) from depth to formation (DF, meters) input data, as shown in equation 3.2. The SWA boundary delineates the start of the calculated positive results (> 0), which means that anything within this SWA boundary is considered for storage. Consideration of the bottom storage window boundary is not necessary, as the formation depth extent cannot exceed the depth to the bottom boundary.

$$SWA = DF - Depth\ to\ top\ boundary \tag{3.3}$$

2. Clip the Formation Thickness (FT) input data utilizing the SWA. The FT input data is then cropped to match the SWT's 2D spatial extent utilizing ArcGIS's Clip tool.

The Gulf of Mexico (GOM) reservoir units are an exception step 1 (above) and do need to consider the bottom window boundary because the GOM's bottom SSW boundary is not the sedimentary rock thickness vertical extent; rather, it is the depth to top of overpressure (refer to section 2.3.4).

3.3.2 AREA

The area under consideration for this spatial database is an arbitrary, standardized area describing the size and extent of the data. Thus, the area utilized to calculate pressure-based capacity stems from the minimum gridded spatial data resolution found from the input data. In this scope of work, that translates to an area of 25,000,000 m^2 or 25 km^2. This remains constant for all data calculations, regardless of the input data.

3.3.3 NET TO GROSS INJECTABLE INTERVAL

Net to Gross (N:G) injectable interval is a geological term used to describe the thickness of permeable, prospective reservoir versus the overall interval thickness. This includes both carbonates and siliciclastic sedimentary rock reservoirs. The N:G injectable interval is usually expressed as a percentage or decimal fraction, with higher values indicating a greater proportion of permeable reservoir to non-permeable reservoir. It is an important parameter used in petroleum geology and reservoir engineering for evaluating the quality and potential productivity of a sedimentary rock or reservoir.

3.3.4 MIDPOINT FORMATION DEPTH

Midpoint formation depth (MPD, meters) is calculated by adding half of the storage window formation thickness (SWFT, meters) parameter to depth to top of formation (DF, meters) input data.

$$MPD = DF + \frac{1}{2}SWFT \quad (3.4)$$

3.3.5 POROSITY

Porosity is defined as the percentage of fluid-filled space within a given volume of rock. Over time, the rock is buried and subjected to increasing pressure, thus undergoing compaction. This process generally leads to a reduction of the volume of the rock and as a result decreases its primary porosity. The amount of compaction and porosity reduction depends on the type of rock, maximum depth of burial, diagenesis, and the temperature and pressure conditions.

3.3.6 RESERVOIR TEMPERATURE

Reservoir temperature is a key parameter to calculate pressure-based CO_2 storage capacity. Other parameters needed for storage capacity calculations, such as CO_2 density (refer to section 3.3.10) and brine compressibility (3.3.9), incorporate reservoir temperature data.

To calculate the reservoir temperature, it is necessary to consider the natural variations in both the Earth's crust and its surface. For example, variations in lithology (i.e.,, sandstone versus granite) and crustal thickness create a range of geothermal gradients throughout the Earth's crust. Surface temperatures throughout the U.S. also experience variations due to seasonal changes and climate. Thus, a regional geothermal gradient data map (Blackwell and Richards, 2004) and an average surface temperature data map (Fick and Hijmans, 2017) were utilized in this reservoir temperature assessment as input data.

The geothermal gradient (G, °C/km), combined with the average surface temperature (T_s, °C) and midpoint formation depth (MPD, meters) make up the reservoir temperature (T_R, °C) (eq. 3.5).

$$T_R = T_s + \frac{MPD}{1000} * G \tag{3.5}$$

3.3.7 SALINITY

Salinity is an important input data parameter because it partly determines the allowable pressure increase within a reservoir. The salinity of a brine determines the brine density, which in turn affects the compressibility of a brine fluid. A higher brine compressibility would lower the total allowable pressure increase within a reservoir. Discussion on the source of data utilized for salinity can be found in section 6.2.6.

3.3.8 PRESSURE INCREASE

Pressure in the subsurface increases with depth due to the stress exerted by an increasing overburden of rock and fluid (i.e., brine water) with depth. A hydrostatic pressure gradient, or the pressure exerted by a column of fluid, increases at around 10.52 MPa/km (0.465 psi/ft) for subsurface brines (Tiab and Donaldson, 2016). A lithostatic pressure gradient, or the stress exerted by layers of rock stacked on top of each other, increases at 22.6 MPa/km (1.0 psi/ft) (Tiab and Donaldson, 2016). To find the hydrostatic (P_H, MPa) or lithostatic pressure (P_L, MPa) at a given depth in a reservoir formation, the Midpoint Formation Depth (MPD, meters) parameter is multiplied by the hydrostatic or lithostatic pressure gradient (Eq. 3.6 and 3.7).

$$P_H = 10.52 * \frac{\text{MPD}}{1000} \tag{3.6}$$

$$P_L = 22.62 * \frac{\text{MPD}}{1000} \tag{3.7}$$

However, pore volume in the subsurface is already saturated with fluid; consequently, the injection of CO_2 for storage purposes within this saturated porous volume can lead to the destabilization and fracturing of the rock if the pore volume becomes overpressured. One method to estimate the pressure at which the rock will fracture due to overpressure is by using Eaton's Method (Eaton and Eaton, 1997), summarized in eq. 3.8 below. Eaton's fracture pressure (P_E) is in units of MPa.

$$P_E = \frac{v}{(1-v)} * (P_L - P_H) + P_H \tag{3.8}$$

To calculate the fracture pressure point, Eaton's Method considers three variables: the lithostatic and hydrostatic pressures as discussed above, and Poisson's ratio (v). Poisson's ratio describes the 2D horizontal to vertical directional stress transmissivity behavior ratio of a rock, with a higher v value indicating that the rock transmits more stress vertically than horizontally. Poisson's ratio typically ranges from -1 to 0.5 (Sokolnikoff, 1983) for different types of solid materials (i.e., metals and minerals), with sandstones, shales, and carbonate rocks averaging around 0.2, 0.3, and 0.3, respectively (SLB Energy Glossary). Analyses on Mt. Simon Formation sandstone cores from the CO_2 sequestration demonstration project at Decatur, IL resulted in a Poisson's ratio between 0.14 to 0.27 (Morrow et al 2017). For simplicity, this scope of work will assume a constant Poisson's ratio of 0.25 for all the given reservoir formations.

The difference between Eaton's fracture pressure and hydrostatic pressure is known as Effective Stress (P_{Ef}, MPa), which translates into the amount of pressure increase within the porous volume required to fracture the rock, as well as the point at which the rock becomes overpressured. Effective Stress is summarized in eq 3.9 below:

$$P_{Ef} = P_E - P_H \tag{3.9}$$

As a precaution to avoid overpressure, the pressure increase (P_I) considered for pressure-based CO_2 storage capacity calculations is only 90% of the calculated Eaton's fracture pressure minus the hydrostatic pressure, as described by eq. 3.10 below.

$$P_I = 0.9 * P_E - P_H \tag{3.10}$$

3.3.9 TOTAL COMPRESSIBILITY

Compressibility is the measure of a fluid or a solid's volume change as a response to pressure changes exerted upon said volume. The porous volume in which the CO_2 is injected and stored will experience increasing pressure, and thus will also be subjected to compressibility. To account for the compressibility of both the fluid ($C_B, \frac{1}{MPa}$) and solid rock unit ($C_R, \frac{1}{MPa}$) in the porous volume as a response to the pressure changes for CO_2 storage capacity calculations, the following relationship is established, where C_T is the total compressibility of the porous volume:

$$C_T = C_R + C_B \tag{3.11}$$

The compressibility of rock and brine calculations are derived from Mathias et al. 2009, who also provide a methodology for estimating pressure buildup due to CO_2 injection for CCS purposes. The equations are as follows:

$$C_R = \frac{0.01411}{(1 + 55.87 * \Phi)^{1.42859}} \tag{3.12}$$

$$C_B = \frac{145}{(7.033 * P_H + 541500 * S - 537 * T_R + 403300)} \quad (3.13)$$

where hydrostatic pressure (P_H) is in psi units, porosity (Φ) is in decimals, and reservoir temperature (T_R) is in degrees Fahrenheit.

3.3.10 CO_2 DENSITY

Calculating the density of a gas or fluid within a reservoir requires consideration of the relationship between pressure, volume, molar mass, and temperature as described by the ideal gas law. The ideal gas law (PV = nRT) assumes that the gas occupies a large volume, and that the intermolecular forces between the particles are negligible. However, at burial temperatures and pressures where CO_2 is stored, the CO_2 is supercritical and the ideal gas law no longer applies.

To account for the behavior of a non-ideal gas under high temperature and pressure conditions, the compressibility factor (Z) is used as a modifier to the ideal gas law. It is a dimensionless number that represents the deviation of the actual volume occupied by a gas from the ideal volume predicted by the ideal gas law since it reflects the effects of intermolecular forces of a gas at a given pressure and temperature. Z values less than 1 indicate that the gas is more compressible than an ideal gas. The ideal gas law with the compressibility factor Z can be rewritten as:

$$Z = \frac{P * V}{R * T} \quad (3.14)$$

$$P = P_A + P_H \quad (3.15)$$

where P is the final pressure in MPa, V is molar volume cm^3, R is the gas constant 8.314 J/mol-K, and T is temperature in Kelvin (K). Allowable pressure increase (P_A) and hydrostatic pressure (P_H) are discussed in section 3.3.8.

Several equations of state to solve for density of a gas given pressure and temperature have been proposed in the past couple centuries, (e.g., van der Waals and Peng-Robinson). For the scope of this thesis, the Peng-Robinson equation of state (Robinson and Peng, 1976) will be utilized to calculate CO_2 density. Solving for Z, the Peng-Robinson equation of state is as follows (Elliot and Lira, 2012):

$$Z = \frac{1}{(1 - B/Z)} - \frac{A}{B} * \frac{B/Z}{1 + \frac{2B}{Z} - (\frac{B}{Z})^2} \tag{3.16}$$

where A and B are dimensionless forms of empirically determined parameters that depend on the properties of the gas. Rearranging eq. 3.16 to solve for Z results in the following cubic Peng-Robinson equation of state:

$$Z^3 - (1 - B) * Z^2 + (A - 3B^2 - 2B) * Z - (AB - B^2 - B^3) = 0 \tag{3.17}$$

With the real solution of Z from eq 3.17, the molar weight of CO_2 (44 g/mol), and a rearranged version of eq. 3.17 to solve for V, CO_2 density ($\rho_{CO2}, \frac{kg}{m^3}$) can be calculated:

$$\rho_{CO2} = \frac{44000 * P}{Z * R * T} \tag{3.18}$$

Chapter 4: CO_2 Injectivity Methodology

4.1 INTRODUCTION

Injectivity is a term used in CCS to describe the ability of a fluid or a gas to be injected into and through a porous volume in the subsurface. The easier it is for the fluid or gas to be able to flow within the porous volume, the higher the rate of injection, which means higher injectivity of said fluid or gas. Injectivity is influenced by several factors, including the physical properties of the geologic reservoir (i.e., permeability and the net to gross injectable interval within the reservoir thickness), the pressure and temperature of the fluid or gas, and the presence of impurities in the fluid or gas.

Quantifying CO_2 injectivity is important for the development of new CCS projects. Quantification of CO_2 injectivity can help determine how many wells are needed per project to reach defined storage goals over time (i.e., 1 million tons of CO_2 is input into the economic feasibility of the project).

4.2 CALCULATING CO_2 INJECTIVITY

Injectivity is usually calculated from field injection and pressure data from a well. Previous injectivity studies (Guo et al. 2008, Valluri et al. 2020) focused on the injectivity index (J) to characterize the capability of a well to inject fluid into a reservoir. Reservoir properties such as permeability, size, and thickness, well properties (diameter and design), skin factor, two phase relative permeability, friction, and pressure drop from the wells are considered. The injectivity index (J) as a radial steady state flow around a vertical well (Guo et al. 2008) is summarized below in eq. 4.1, where k is permeability, h is thickness, and the denominator variables are related to the formation and bottom hole pressure:

$$J = \frac{q}{(p_e - p_{wf})} = \frac{k * h}{141.2 * B_o * \mu_o * \left(ln\frac{r_e}{r_w} + S\right)} \quad (4.1)$$

However, well pressure data is not readily available at a regional level, and so the injectivity calculations for this scope of work have been simplified to depend solely on the permeability and thickness of the reservoir. Previous work has demonstrated that injectivity calculations based on permeability and thickness are a good, simplified proxy to the injectivity index, since the relationship between injectivity and permeability/thickness is linear (Hoffman et al. 2015, Valluri et al. 2020).

Thus, in this study, injectivity (I) is estimated by multiplying the permeability (k, millidarcy) of the porous volume by the storage window formation thickness (SWFT, meters) and the net to gross injectable interval (N:G) as shown in eq. 4.2 below. Injectivity is in units of millidarcy-meters, which is abbreviated as mD-m.

$$\mathrm{I} = k * SWFT * N{:}G \quad (4.2)$$

4.3 CO_2 Injectivity Parameters

SWFT and N:G are also CO_2 storage cost estimation input parameters, which have been discussed in detail in sections 3.3.1 and 3.3.3, respectively. The remaining parameter, permeability, will be discussed below.

4.3.1 Permeability

Permeability of a rock refers to the ability of a rock to allow fluids, such as water or gases, to pass through it. It is a measure of the pressure drop required to drive fluid flow through a material. Permeability plays a critical role in various natural processes, including

groundwater movement, oil and gas extraction, and carbon storage and sequestration (CCS).

In the context of CCS, permeability is a crucial factor that affects the success of CCS projects. Permeable materials, such as porous sandstones and fractured rocks allow CO2 to be injected into storage reservoirs. Layers of less permeable materials, such as shales, act as barriers to vertical migration of buoyant CO2, retaining it in the reservoir. Therefore, understanding the permeability of rocks in potential storage sites is essential for identifying suitable locations for injection and ensuring the long-term retention and effectiveness of CO_2 storage projects.

Chapter 5: CCS Project Storage Cost Analysis Methodology

5.1 INTRODUCTION

This chapter focuses on calculating storage costs based on the optimized pressure-based capacity and injectivity calculations defined in chapters 3 and 4, respectively. The conversion from capacity and injectivity into costs are based on equations developed by Dr. Bump (Bump 2023, written communication), while the storage costs are based on a new cost methodology (Hovorka 2023, written communication). The equations utilized, as well as both methodologies, are briefly summarized in this chapter.

It is important to clarify that the storage costs calculated in this analysis assume a constant capacity of 20 Mt, where 1 million metric tons per year (Mtpa) are injected throughout a 20-year project timeframe. This simplification setting of a project scale and duration is novel and allowed for the analysis of the area needed per project (pressure space).

5.2 TRANSLATING PRESSURE-BASED CAPACITY AND INJECTIVITY INTO COST

To quantify storage costs per project, there are two main concepts derived from pressure-based capacity and injectivity results: 1) Area per project and 2) Wells needed to inject 1 Mtpa. Area per Project is specifically derived from the quantification of capacity in a given area, whereas the wells needed to inject a certain rate are directly related to the injectivity available within the same area.

5.2.1 AREA PER PROJECT

The Area per Project in this scope of work describes the total area necessary to develop a CCS project that aims to store 20 Mt of CO_2 at a 1 Mtpa rate for 20 years. To calculate the area per project, the capacity per area needs to be calculated first.

Capacity per area ($Cap_{Area}, \frac{MMT}{km^2}$) is the result from dividing the pressure-based capacity (Cap_{PS}, Mt) calculated in section 0 by the area (A, in km^2) defined in section 3.3.2, which converts capacity into a calculation that varies spatially per 1 km^2 area. Capacity per area is summarized in eq. 5.1 below:

$$Cap_{Area} = \frac{Cap_{PS}}{A} \tag{5.1}$$

The area per project (A_{Proj}, km^2) is then calculated by dividing the total capacity of 20 Mt by the capacity per area, as shown below in eq. 5.2:

$$A_{Proj} = \frac{20}{Cap_{Area}} \tag{5.2}$$

5.2.2 NUMBER OF WELLS NEEDED TO INJECT 1 MTPA

The calculation to get the number of wells needed to inject 1 Mtpa is based on the simplifying assumptions presented in the paper authored by Hoffman et al. (2015). The results presented in Hoffman's paper show different injectivity thresholds per injectivity rate, which included a minimum of 10,000 mD-m to be able to inject 1 Mtpa within a reservoir. The threshold classification stems from reservoir injectivity quality based on onshore CCS research projects, such as Decatur (Gollakota and McDonald, 2014) and Cranfield (Hovorka, 2013). Thus, the number of wells (*Wells*) needed to inject 1 Mtpa is calculated by rounding up to the nearest integer the result from dividing Hoffman's 1 Mtpa injectivity threshold by the calculated injectivity (I, mD-m):

$$Wells = \left\lceil \frac{10000}{I} \right\rceil \quad (5.3)$$

5.3 CCS PROJECT STORAGE COSTS

As part of this study, a new storage cost calculation methodology (Hovorka 2023, written communication) is based on the area per project (A_{Proj}), derived from the optimized pressure-based capacity calculations, and number of wells (*Wells*), derived from optimized injectivity calculations. This new storage cost methodology results in both storage costs per project and storage costs per ton of CO_2. Note that the costs only consider storage-related costs and do not consider capture nor potential transportation costs.

5.3.1 STORAGE COSTS PER PROJECT

The new storage cost methodology takes into consideration different cost categories, including the costs of development, exploration, monitoring, closure, and general benefits to the community from a CCS project. For each category, there are separate cost items to be considered. For example, exploration may include 2-D and/or 3-D seismic surveys costs based on distance per survey. Table 5.1 summarizes the costs per category defined by Hovorka 2023, written communication.

Category	Abbr.	Item	Cost ($ USD)
Development	D	Injection well per 1 well	$ 3,725,000.00/well
Exploration	E_{2D}	2-D seismic survey, per km, per line	$15,625.00/km
	E_{3D}	3-D seismic Survey per km^2	$100,000.00/ km^2
Monitoring	M	Monitoring per km^2 of project area for 20 years	$8,580,00.00/ km^2
Pore Space Lease	PS	Pore-space lease per km^2	$7,500.00/ km^2
	PS_b	Bonus per km^2 for 20 years	$2,000.00/$km^2$
	PS_L	Landowner fee per ton of CO_2	$3.00/ton
Closure	C	Insurance and closure fee per ton of CO_2	$0.10/ton
Community benefits	C_B	Community benefits fee per ton of CO_2	$0.10/ton

Table 5.1: Storage costs per project as defined by the methodology from (Hovorka 2023, written communication)

The storage costs per project, in units of $ MM USD (millions of US dollars) , are then calculated by adding all cost categories together, as indicated in eq. 5.4 below.

$$Storage\ Costs\ per\ Project = Dev + Exp + Mon + Lease + Closure + Community \quad (5.4)$$

$$Dev = Wells * D \quad (5.4a)$$

$$Exp = \left(\sqrt{A}_{Proj} + 2\right) * E_{2D} + 2 * ((A_{Proj} * 0.05) + 6) * E_{3D} \quad (5.4b)$$

$$Mon = \left(\frac{A_{Proj}}{100}\right) * M + M \quad (5.4c)$$

$$Lease = ((A_{Proj} * 0.05) + 4) * (PS + PS_B) + 20{,}000{,}000 * PS_L \quad (5.4d)$$

$$Closure = 20{,}000{,}000 * C \quad (5.4e)$$

$$Community = 20{,}000{,}000 * C_B \quad (5.4f)$$

5.3.2 CO_2 Storage Costs per Ton

To calculate storage costs per ton, the total storage costs per project are divided by the assumed CO_2 injection rate per year and the expected longevity of the project, which are 1 Mtpa and 20 years. Units of storage costs are in $USD per ton of CO_2.

$$Storage\ Costs\ per\ ton = \left\lceil \frac{Storage\ Costs\ per\ Project}{20\ yr * 1{,}000{,}000\ tons\ per\ year} \right\rceil \quad (5.5)$$

5.3.3 Consideration of Costs within the Storage Window

For areas where storage potential exists but the geologic data parameters used to calculate capacity and injectivity do not exist, we estimate storage costs based on the statistical results from areas where storage costs are available and were calculated. In addition to storage costs per project detailed in eq 5.4, the new storage costs for the storage window consider additional 2-D seismic exploration costs, as well as additional exploration

wells required to find a viable site. We assume the exploration and injection wells costs (D) are equal. The 90th percentile (P90) of the storage costs per project results, as well as the 90th percentile of the area of project results are utilized as the "worst" case cost scenarios for these areas. Thus, the storage costs per project within the storage window can be calculated as indicated in eq. 5.6. Additionally, the storage costs per ton calculation (e. 5.5) remain the same for these areas where no geologic data exists.

$$\frac{Storage\ Costs\ in}{Storage\ Window} = P90\ (Storage\ Costs\ per\ Project) + 2 * \left[\left(P50\left(\sqrt{A}_{Proj}\right) + 2\right) * E_{2D}\right] + 3 * D \quad (5.6)$$

Chapter 6: CO_2 Capacity, Injectivity, and Cost database

6.1 INTRODUCTION

As part of the scope of work and final deliverable of this thesis, a nationwide "*CO_2 Capacity, Injectivity, and Cost*" database was created based on the methodologies described in Chapters 3 through 5. This chapter goes over the acquisition and description of the different sources of data used to calculate pressure-based capacity, injectivity and storage costs per ton for a list of available reservoirs throughout the U.S., as well as the processing of said different sources of data to one unified dataset. Further on, this chapter also describes the structure of the database created for this thesis, as well as introducing a data quality ranking comparing the different sources of data utilized to create the database. The data acquisition and processing of the sedimentary CO_2 storage window data summarized in Chapter 2 are not discussed in this chapter.

6.2 DATA ACQUISITION

There are two main sources of data utilized to calculate and create the "*CO_2 Capacity, Injectivity, and Cost*" database, which includes the U.S. Geological Survey's (USGS) Carbon Dioxide Storage Assessment database (USGS, 2013) and the Gulf Coast Carbon Center's (GCCC) CO2 Brine Database (GCCC, 2012). Each of the datasets are pioneering work aimed to show that the volumes that could be injected into the subsurface are sufficient at scales relevant to climate change reduction and the overall favorable deployment of CCS across the U.S.

Both the USGS and the GCCC's original databases lack some of the data needed to calculate capacity and injectivity (i.e., salinity) and so require supplementary sources of data to complete the datasets. Supplemental data sources and methodologies are discussed

in this chapter. Table 6.1 summarizes the data availability for both the GCCC and USGS data sources.

Input Data	Abbreviation	GCCC ID	Supplementary Data Section	USGS ID	Supplementary Data Section
Depth to Formation	DF	001	N/A	Depth to SAU	N/A
Formation Thickness	FT	003	N/A	SAU Thickness	N/A
Area	A	N/D	3.3.2	SAU Spatial Area	3.3.2
Porosity	Φ	014	6.2.2	Net Porous	N/A
Permeability	k	002	6.2.2	Permeability	N/A
Salinity	S	012c	0	N/D	N/A
Net to Gross Ratio	N:G	N/D	6.2.2	Net Porous Thickness	N/A
Surface Temperature	T_S	N/D	6.2.3	N/D	6.2.3
Geothermal Gradient	G	N/D	6.2.5	N/D	6.2.5
Poisson Ratio	v	N/D	6.2.7	N/D	6.2.7

Table 6.1: GCCC and USGS Input Data original data IDs, availability, and supplementary data source /methodology considered for this scope of work. Each supplementary data source is described in detail in different sections throughout the thesis. N/D = no data available or taken from this source. N/A = Not Applicable. SAU = Storage Assessment Unit, used in USGS, 2013 study as a reservoir metric.

6.2.1 GCCC CO_2 BRINE DATABASE

The CO_2 Brine database from the Gulf Coast Carbon Center (GCCC) contains gridded data for 25 different geologic reservoirs within US sedimentary basins that have been identified to have CO_2 storage feasibility. One of the advantages of having gridded data is that it provides continuous, high-spatial resolution data over a surface, which means the quantity and resolution of the data is much better than, for example, a point or contour type of data.

The database contains more data that was utilized in this study's scope of work. For the sake of simplicity and data compatibility with other sources the only data utilized are: 1) Depth to Formation (DF), 2) Formation Thickness (FT), 3) Porosity (Φ), 4) Permeability (k), and 5) Salinity (S). It is important to note that permeability values were capped at 300 mD for all formations.

The type of data between the five data sources varies between gridded data and single average data values. For example, depth and thickness of formation for all 25 reservoirs are gridded data. As for porosity, permeability, and salinity, the data ranges between single values to gridded data, with some data gaps. Table 6.2 below summarizes the type of data and data values for all GCCC's 25 reservoirs.

GCCC ID	System ID	Basin	System	GCCC Reservoir Name	Porosity (Φ)	Permeability (k)	Salinity (S)
1	3	Anadarko and Southern Oklahoma Basins	Cambrian	Arbuckle Group	0.03	1	9999
2	10	Appalachian Basin	Devonian	Oriskany Sandstone	9999	9999	9999
3	14	Atlantic Coastal Plain	Cretaceous	Lower Potomac Group	0.20	300	N/D
4	14	Atlantic Coastal Plain	Cretaceous	Cape Fear	0.20	300	N/D
5	14	Atlantic Coastal Plain	Cretaceous	Tuscaloosa	9999	300	N/D
6	21	Black Warrior Basin	Mississippian	Pottsville	0.10	N/D	9999
7	22	Denver Basin	Permian	Lyons Sandstone	N/D	N/D	N/D
8	31	Illinois Basin	Ordovician	St. Peter	N/D	N/D	9999
9	36	Los Angeles Basin	Miocene	Repetto	0.25	N/D	9999
10	37	Michigan Basin	Ordovician-Cambrian	Mt. Simon	N/D	N/D	N/D
11	41	Palo Duro Basin	Paleozoic	Granite Wash	N/D	N/D	N/D
12	44	Permian Basin	Permian	Dean	9999	N/D	N/D
13	44	Permian Basin	Permian	Queen	9999	N/D	N/D
14	44	Permian Basin	Permian	San Andres	9999	N/D	N/D
15	44	Permian Basin	Permian	Spraberry	9999	N/D	N/D
16	44	Permian Basin	Permian	Wolfcamp	9999	N/D	N/D
17	44	Permian Basin	Permian	Yates	9999	N/D	N/D
18	45	Powder River Basin	Cretaceous	Fox Hills	0.21	50	N/D
19	54	San Juan Basin	Jurassic	Morrison	N/D	N/D	N/D
20	56	South Florida Basin	Cretaceous	Cedar Keys	0.25	20	9999
21	58	U.S. Gulf Coast	Oligocene	Oligocene	0.22	N/D	N/D
22	61	U.S. Gulf Coast	Cretaceous	Woodbine	9999	9999	9999
23	61	U.S. Gulf Coast	Cretaceous	Paluxy Sand	9999	N/D	N/D
24	57	U.S. Gulf Coast	Eocene	Wilcox Group	0.25	N/D	N/D
25	69	Williston Basin	Carboniferous	Madison Group	0.10	N/D	N/D

Table 6.2: GCCC porosity, permeability and salinity input data. Inputs marked with 9999 indicate that the data provided is in a gridded format. N/D = No Data.

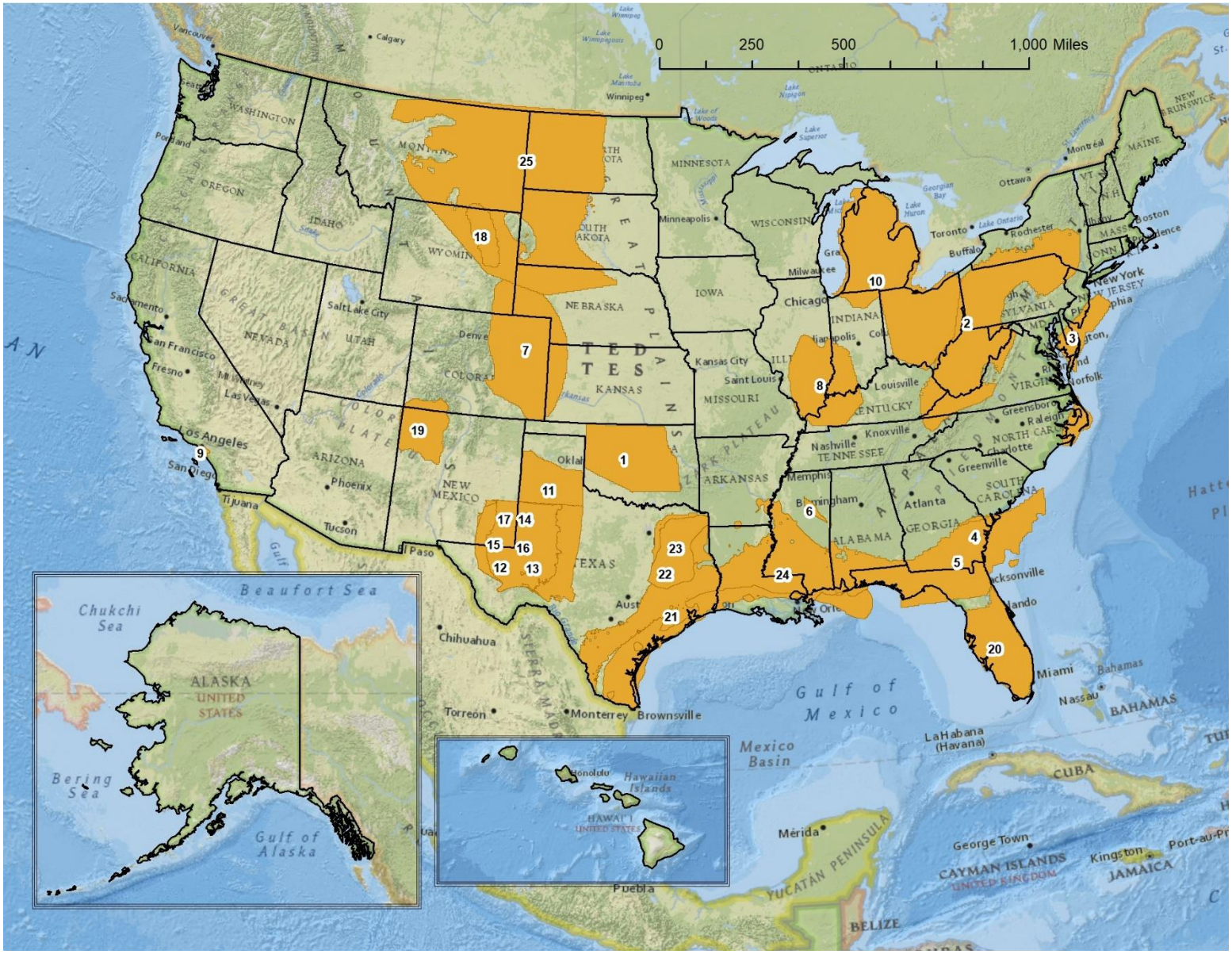

Figure 6.1: GCCC's CO2 Brine database 25 reservoir spatial data extent (GCCC, 2012). Refer to Table 6.2 for reservoir labels.

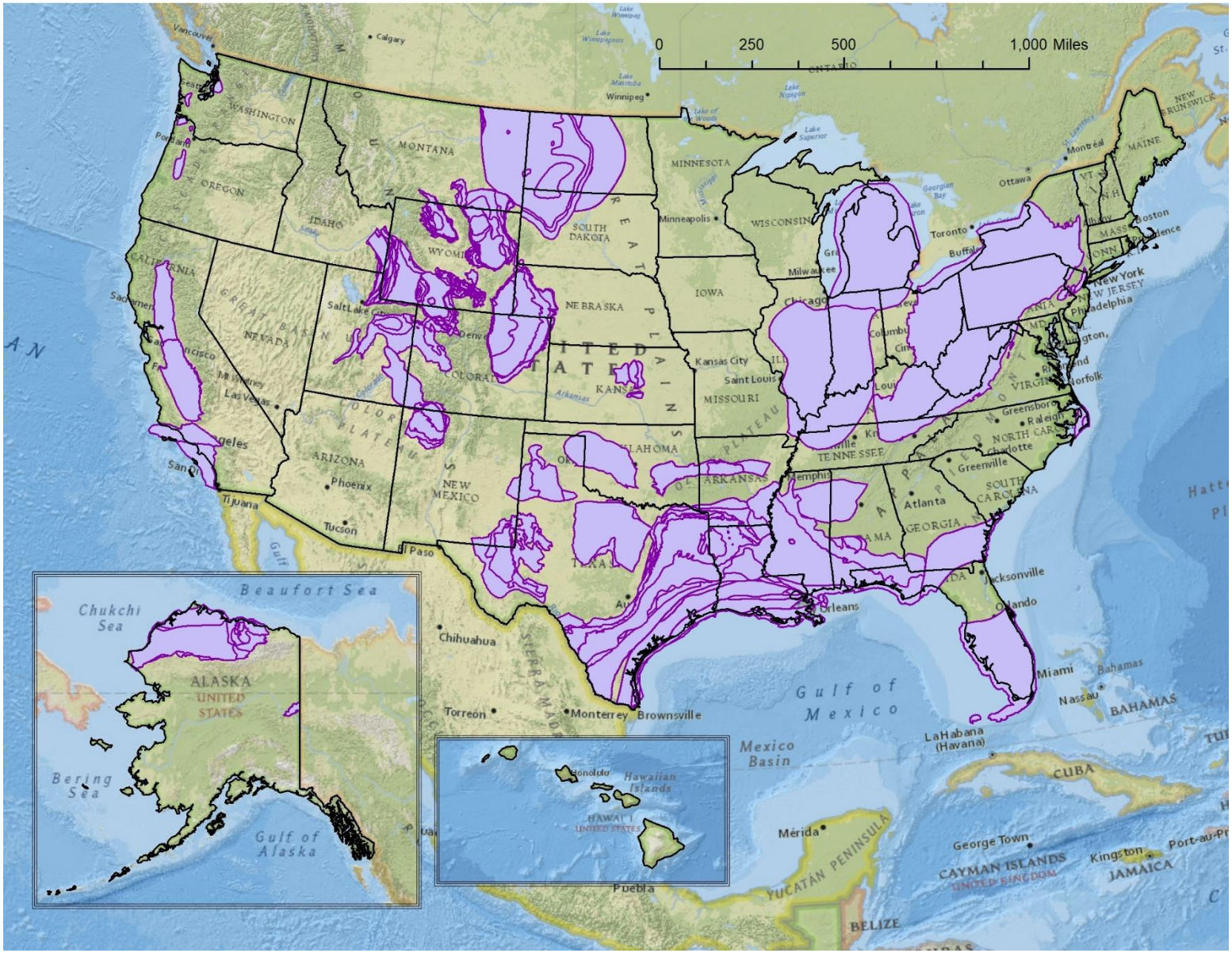

Figure 6.2: USGS's Carbon Dioxide Storage Assessment spatial data extents (USGS, 2013).

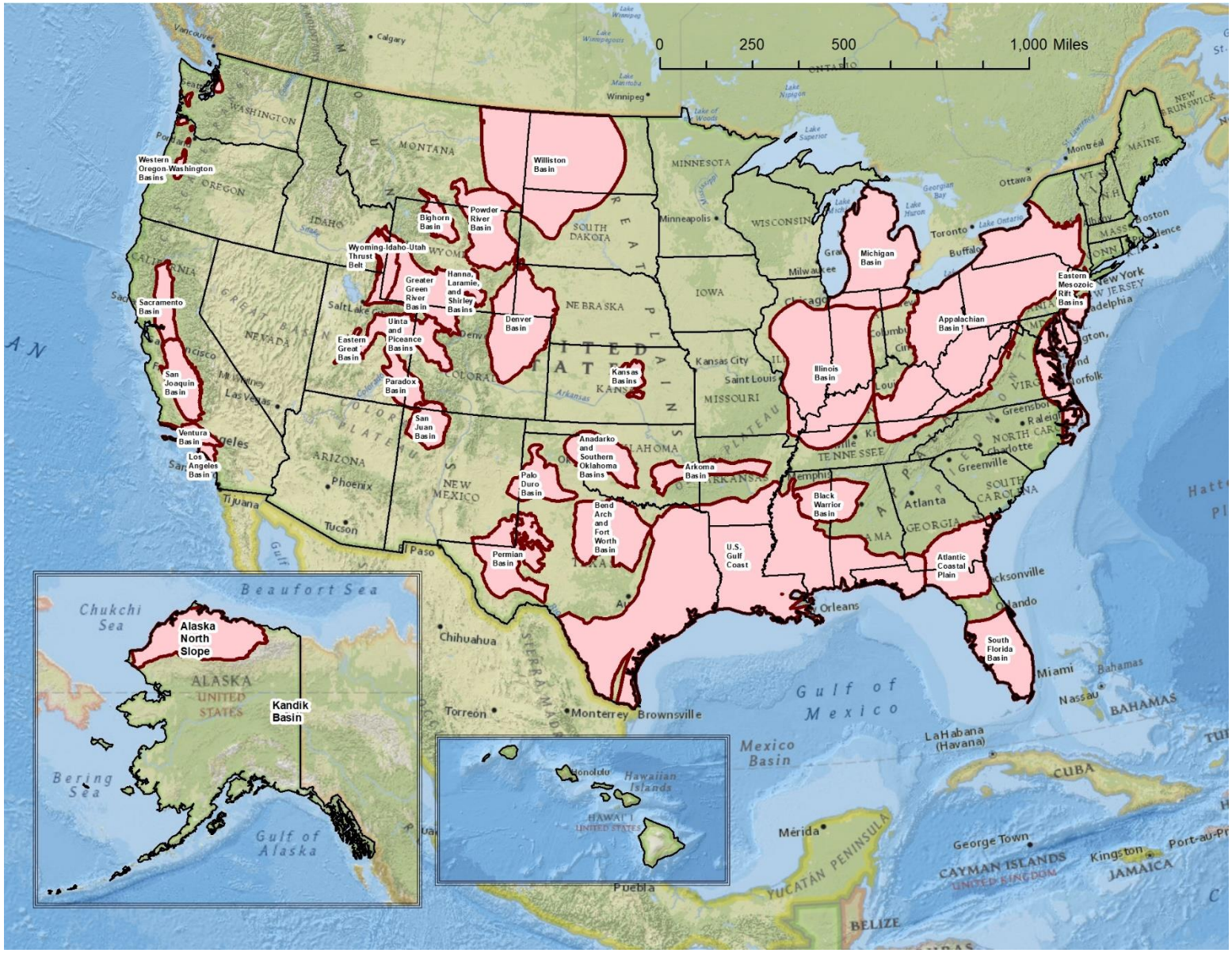

Figure 6.3: USGS Basin extents compiled from USGS Carbon Dioxide Storage Assessment (USGS, 2013)

6.2.2 U.S. GEOLOGICAL SURVEY CARBON DIOXIDE STORAGE ASSESSMENT

In 2013, the U.S. Geological Survey released their Carbon Dioxide Storage Assessment report and database (USGS, 2013) in which they identified and analyzed 192 potential CO_2 storage assessment units (SAU) within 32 sedimentary basins in the U.S. A SAU can either be a single geologic formation or a grouping of formations identified to be favorable for CO_2 storage. Part of their assessment consisted of averaging porosity and permeability well data to calculate static (volumetric) CO_2 capacity for each SAU. The resulting database consists of spatial (polygon) and tabular data where each SAU has one single value of input data (i.e., depth to formation, porosity, formation thickness, etc.) per SAU. The data utilized by the USGS originates form the Nehring Associates' oil and gas database (Nehring Associates Inc, 2012)

In some cases, the USGS database provided supplementary porosity, permeability, and N:G data to the GCCC database. The single value porosity and permeability values from the SAUs are applied to either the partial or entire extent of the GCCC spatial data. Section 6.3.2 delves more into details.

6.2.3 USGS BASIN EXTENT DATA

The USGS basin extent data is extracted from the USGS's Carbon Dioxide Storage Assessment database. The USGS's SAU spatial extent data were combined to create the basin extents as mapped in Figure 6.3. The SAUs pending publication (e.g., such as the ones found within the Illinois, Michigan, and Appalachian Basins) were substituted by the USGS Total Petroleum Assessment spatial data for these basins.

6.2.4 SURFACE TEMPERATURE

The surface temperature dataset utilized in this scope of work stems from the work from Fick and Hijmans (2017) on an annual mean surface temperature gridded dataset. The weather data was collected from between 9,000 to 60,000 weather stations between the years 1970 and 2000. For areas with low station density, the study utilized satellite data to compensate for any lack of data. Surface temperature is important to calculate the reservoir temperature, as explained in section 3.3.6 and summarized by equation 3.5.

To find the surface temperature for each potential CO_2 storage reservoir, an average measure of the mean surface temperature was calculated by utilizing the basin extents and the ArcGIS zonal statistic tool. This tool takes spatial data and outputs statistics from the data within the spatial extent. Thus, either a reservoir from GCCC's database or an USGS SAU within the same basin contains the same surface temperature data points.

6.2.5 GEOTHERMAL GRADIENT

The geothermal gradients utilized in this scope of work originate from the work done within the SMU geothermal lab (Blackwell and Richards, 2004). As with surface temperature, the geothermal gradient is an important input for calculating reservoir temperature (refer to section 3.3.6 and eq. 3.5).

Although Blackwell and Richards (2004) do provide the original well data to calculate a geothermal gradient gridded dataset, they did not publish the gridded dataset itself. Only image maps are available for the public to use. So, the U.S. Blackwell and Richards (2004) geothermal gradient map was georeferenced to fit the extent of the conterminous U.S. in ArcGIS Pro. The basin extent data were then overlaid on the georeferenced geothermal map to estimate the geothermal gradient on a basin-wide level. Both the USGS and GCCC's databases share the same geothermal gradient values per basin

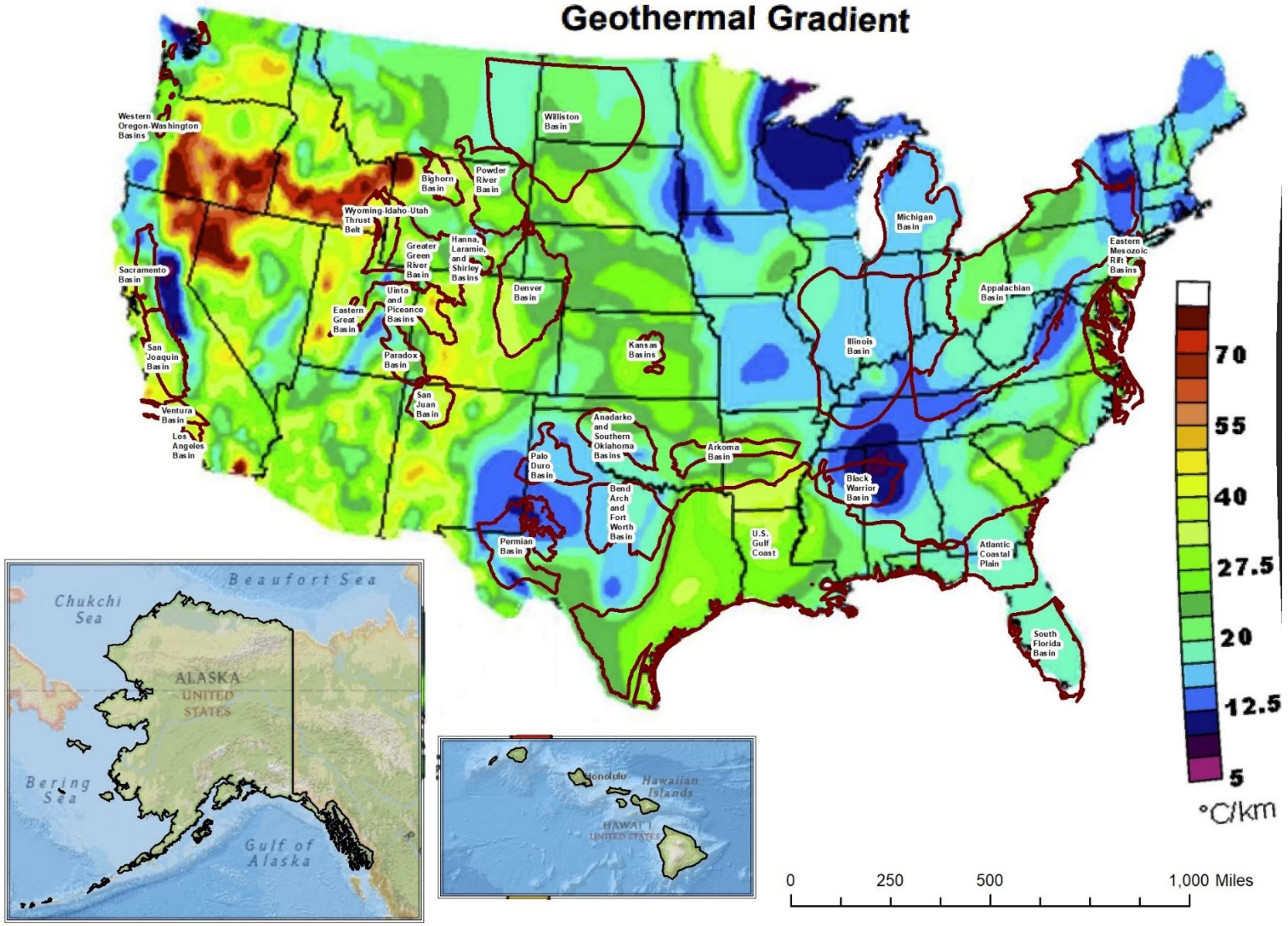

Figure 6.4: The 32 Sedimentary Basins considered for CO2 Storage overlaying the Geothermal Gradient map from the SMU Geothermal Lab (Blackwell and Richards, 2004).

6.2.6 SALINITY

For the scope of this study and for areas with no salinity data available, salinity is based on Ferguson et al. (2018). Geologic reservoirs within sedimentary basins tend to have low structural relief. Ferguson et al. (2018) investigated the driving force ratio (DFR) found within the structural relief of said geologic reservoirs relative to basin depth and found that this ratio predicts the presence of stagnant brines within the reservoir. A higher DFR ratio indicates a lower topographic relief within a basin and a higher salinity concentration. The paper concludes that basins with DFR > 1 contain brines with a saline concentration of over 0.1 kg/L. Thus, basins with a DFR>1 are represented with a value for salinity of 0.12 kg/L, while basins with a DFR < 1 are represented with a salinity of 0.08 kg/L.

6.2.7 POISSON RATIO

Poisson's ratio typically ranges from -1 to 0.5 (Sokolnikoff, 1983) for different types of solid materials (i.e., metals and minerals), with sandstones, shales, and carbonate rocks averaging around 0.2, 0.3, and 0.3, respectively (SLB Energy Glossary). Analyses on the Mt. Simon Formation sandstone cores from the CO_2 sequestration demonstration project at Decatur, IL resulted in a Poisson's ratio between 0.14 to 0.27 (Morrow et al 2017). For simplicity, this scope of work assumes constant Poisson's ratio of 0.25 for all the given reservoir formations.

6.3 DATA PROCESSING

One of the bigger challenges when creating the "*CO_2 Capacity, Injectivity, and Cost*" database was processing and unifying datasets that do not match with one another. For example, the GCCC's database gridded data type did not match the spatial extent nor

the resolution of the USGS formation-wide single data values. This subchapter explores how the GCCC and USGS's databases were altered individually first before merging into one single database.

6.3.1 CONSOLIDATING USGS DATA

The first step in unifying the USGS and the GCCC's databases was to consolidate the 182 SAU formations into a total of 74 Systems. The Systems category is already in place in the USGS's original database, and it is based on the SAU's geologic age. The data per SAU was consolidated either by summing the data values per SAU (i.e., Storage Window Formation Thickness, and Net Porous Thickness), averaging the data (i.e., Depth to Formation), or generating a weighted average of the data values (i.e., porosity and permeability). Table 6.3 summarizes the resulting values from consolidating the USGS database from SAU-based to System-based.

The N:G values are derived from the newly consolidated System-based Storage Window Formation Thickness (SWFT, meters) and Net Porous Thickness data (NST, meters), as seen in the relationship below:

$$N{:}G = \frac{NST}{SWFT} \tag{6.1}$$

It is important to note that N:G values were capped at 30% for all Systems. This was done to remove apparent sampling error in some basins which reported thick prospective storage formations but N:G was also high, suggesting that it was based on measurement only in intervals favorable for injection.

System ID	Basin	System	DF (m)	SWFT (m)	MPD (m)	NG (%)	Porosity	Perm (mD)	Surf Temp (°C)	GeothGrad (°C/km)	Salinity (kg/L)
1	Alaska North Slope	Carboniferous	3700	500	3959	14	0.13	46.85	-10.76	25	0.08
2	Alaska North Slope	Cretaceous	1757	500	2007	20	0.13	12.99	-10.76	25	0.08
3	Anadarko and Southern Oklahoma Basins	Cambrian	3962	500	4953	10	0.03	1	14.88	30	0.12
4	Anadarko and Southern Oklahoma Basins	Devonian	3810	125	3924	10	0.08	3.91	14.88	30	0.12
5	Anadarko and Southern Oklahoma Basins	Mississippian	3399	300	4191	10	0.10	13.12	14.88	30	0.12
6	Anadarko and Southern Oklahoma Basins	Permian	1471	500	1737	10	0.13	5.75	14.88	15	0.12
7	Appalachian Basin	Ordovician-Cambrian	2286	610	2591	5	0.08	3.00	9.88	25	0.12
8	Appalachian Basin	Lower Silurian	2286	61	2316	50	0.09	13.00	9.88	25	0.12
9	Appalachian Basin	Upper Silurian	2134	76	2172	12	0.10	16.00	9.88	25	0.12
10	Appalachian Basin	Devonian	2134	61	2164	10	0.07	1.00	9.88	25	0.12
11	Arkoma Basin	Ordovician	2438	1433	3155	23	0.10	10.00	16.09	30	0.12
12	Arkoma Basin	Silurian - Devonian	2438	82	2479	11	0.07	5.00	16.09	30	0.12
13	Arkoma Basin	Carboniferous	2743	76	2781	4	0.11	10.00	16.09	30	0.12
14	Atlantic Coastal Plain	Cretaceous	1003	696	1351	30	0.26	818.41	16.88	20	0.12
15	Bend Arch and Fort Worth Basin	Ordovician - Mississippian	1372	610	1677	15	0.10	1.00	17.89	20	0.08
16	Bend Arch and Fort Worth Basin	Carboniferous	1753	122	1814	30	0.12	25.00	17.89	20	0.08
17	Bighorn Basin	Pennsylvanian	3536	83	3578	30	0.10	35.04	6.50	40	0.08
18	Bighorn Basin	Permian	3506	36	3524	30	0.07	5.50	6.50	40	0.08
19	Bighorn Basin	Triassic	3506	36	3524	30	0.11	5.50	6.50	40	0.08
20	Bighorn Basin	Cretaceous	2835	594	3132	25	0.11	20.03	6.50	40	0.08
21	Black Warrior Basin	Mississippian	1829	198	1928	8	0.10	20.00	16.26	15	0.12
22	Denver Basin	Cretaceous	1691	401	1891	20	0.13	37.67	8.83	30	0.08
23	Eastern Great Basin	Jurassic	2134	427	2348	29	0.08	1.00	8.42	30	0.08

System ID	Basin	System	DF (m)	SWFT (m)	MPD (m)	NG (%)	Porosity	Perm (mD)	Surf Temp (°C)	GeothGrad (°C/km)	Salinity (kg/L)
24	Eastern Mesozoic Rift Basins	Triassic	2286	914	2743	18	0.07	1.00	9.00	20	0.08
25	Greater Green River Basin	Paleozoic	3800	671	4135	10	0.07	1.00	4.62	40	0.08
26	Greater Green River Basin	Triassic-Jurassic	3597	200	3697	30	0.11	5.35	4.62	40	0.08
27	Greater Green River Basin	Cretaceous	3345	150	3420	15	0.10	2.31	4.62	40	0.08
28	Hanna, Laramie, and Shirley Basins	Paleozoic	3963	396	4161	30	0.09	46.76	5.65	30	0.08
29	Hanna, Laramie, and Shirley Basins	Cretaceous	3963	200	4063	23	0.10	19.16	5.65	30	0.08
30	Illinois Basin	Cambrian	1372	366	1554	30	0.11	20.00	12.09	20	0.12
31	Illinois Basin	Ordovician	1417	300	1567	30	0.09	10.00	12.09	20	0.12
32	Illinois Basin	Devonian-Silurian	1250	335	1417	22	0.08	10.00	12.09	20	0.12
33	Kandik Basin	Devonian	1829	500	2079	25	0.10	1.00	-6.21	25	0.12
34	Kandik Basin	Permian	1219	400	1419	25	0.10	1.00	-6.21	25	0.12
35	Kansas Basins	Paleozoic	1015	159	1095	30	0.10	10.00	12.65	13	0.12
36	Los Angeles Basin	Miocene	1219	1829	2134	16	0.17	200.00	17.68	40	0.12
37	Michigan Basin	Ordovician-Cambrian	1981	500	2231	20	0.09	10.00	8.05	20	0.12
38	Michigan Basin	Silurian	1554	335	1722	21	0.07	10.00	8.05	20	0.12
39	Michigan Basin	Devonian	1067	84	1109	18	0.09	10.00	8.05	20	0.12
40	Palo Duro Basin	Paleozoic	1722	1707	2576	10	0.13	81.33	14.06	20	0.08
41	Palo Duro Basin	Permian	1128	762	1509	12	0.15	20.00	14.06	20	0.08
42	Paradox Basin	Paleozoic	2438	762	2819	12	0.10	1.00	9.79	30	0.08
43	Permian Basin	Paleozoic	3871	1341	4542	30	0.07	30.56	15.64	20	0.08
44	Permian Basin	Permian	1524	2286	2667	15	0.14	11.00	15.64	20	0.08
45	Powder River Basin	Pennsylvanian	2743	122	2804	25	0.16	100.00	7.38	30	0.08
46	Powder River Basin	Triassic	1524	27	1538	30	0.13	10.00	7.38	30	0.08
47	Powder River Basin	Jurassic	2035	15	2043	30	0.20	100.00	7.38	30	0.08

System ID	Basin	System	DF (m)	SWFT (m)	MPD (m)	NG (%)	Porosity	Perm (mD)	Surf Temp (°C)	GeothGrad (°C/km)	Salinity (kg/L)
48	Powder River Basin	Cretaceous	1901	589	2195	30	0.20	76.95	7.38	30	0.08
48	Sacramento Basin	Cretaceous	1676	1463	2408	30	0.28	158.89	16.26	16	0.08
50	Sacramento Basin	Eocene	1219	152	1295	30	0.25	200.00	16.26	25	0.08
51	San Joaquin Basin	Cretaceous	2743	975	3231	30	0.27	100.00	16.71	25	0.08
52	San Joaquin Basin	Oligocene	2868	1707	3722	30	0.16	77.86	16.71	25	0.08
53	San Joaquin Basin	Miocene	3482	1341	4153	30	0.17	100.50	16.71	25	0.08
54	San Juan Basin	Jurassic	1829	76	1867	50	0.23	370.00	8.95	40	0.08
55	San Juan Basin	Cretaceous	1552	786	1945	10	0.10	10.55	9.33	40	0.08
56	South Florida Basin	Cretaceous	2841	800	3241	20	0.14	15.00	21.97	25	0.12
57	U.S. Gulf Coast	Eocene	1722	1919	2682	23	0.25	114.81	20.93	35	0.12
58	U.S. Gulf Coast	Oligocene	2134	823	2546	30	0.22	200.00	20.93	35	0.12
59	U.S. Gulf Coast	Miocene	2438	3566	4221	27	0.28	500.00	20.93	35	0.12
60	U.S. Gulf Coast	Jurassic	3843	594	4140	30	0.10	28.57	20.93	35	0.12
61	U.S. Gulf Coast	Cretaceous	2511	3017	4020	20	0.14	40.38	20.93	35	0.12
62	Uinta and Piceance Basins	Paleozoic	3506	1981	4496	28	0.08	1.00	7.00	40	0.08
63	Uinta and Piceance Basins	Cretaceous	3391	191	3487	27	0.11	1.00	7.00	40	0.08
64	Uinta and Piceance Basins	Tertiary	1676	1676	2514	30	0.09	1.00	7.00	40	0.08
65	Ventura Basin	Oligocene	1981	914	2438	33	0.22	100.00	15.04	30	0.08
66	Western Oregon-Washington Basins	Paleogene	1219	1524	1981	30	0.20	200.00	10.63	25	0.08
67	Williston Basin	Cambrian and Ordovician	2820	427	3033	30	0.06	6.51	14.22	20	0.08
68	Williston Basin	Devonian	2698	778	3087	30	0.12	14.48	14.22	20	0.08
69	Williston Basin	Carboniferous	2088	694	2435	17	0.11	14.22	14.22	20	0.08
70	Williston Basin	Jurassic	1676	107	1730	20	0.17	100.00	14.22	20	0.08
71	Williston Basin	Cretaceous	1448	94	1495	30	0.18	88.46	14.22	20	0.08

System ID	Basin	System	DF (m)	SWFT (m)	MPD (m)	NG (%)	Porosity	Perm (mD)	Surf Temp (°C)	GeothGrad (°C/km)	Salinity (kg/L)
72	Wyoming-Idaho-Utah Thrust Belt	Paleozoic	4313	1000	4813	30	0.07	1.54	3.22	45	0.08
73	Wyoming-Idaho-Utah Thrust Belt	Triassic-Jurassic	4115	580	4405	25	0.11	15.00	3.22	45	0.08
74	Wyoming-Idaho-Utah Thrust Belt	Cretaceous	3316	1000	3816	12	0.10	1.00	3.22	45	0.08

Table 6.3: Consolidated USGS Data input from SAU based to System based. DF = Depth to Formation (in meters). SWFT = Storage Window Formation Thickness (in meters). MPD = midpoint depth (in meters). NG = Net to Gross Ratio (%). Perm = Permeability (in millidarcies). GeothGrad = geothermal gradient (in °C/km).

6.3.2 COMPLETING GCCC DATA

The GCCC's CO_2 Brine database was completed by either taking the supplementary data from the USGS's database or from external sources. For example, the N:G, porosity and permeability supplementary values assigned to the GCCC database were taken from the corresponding Systems in the USGS data. Table 6.4 summarizes the original and supplementary data assigned to each reservoir, including the data sources.

GCCC ID	System ID	Basin	System	GCCC Reservoir Name	NG (%)	Porosity	Perm (mD)	Surf Temp (°C)	GeothGrad (°C/km)	Salinity (kg/L)
1	3	Anadarko and Southern Oklahoma Basins	Cambrian	Arbuckle Group	10**	0.03*	1*	14.88^	30^	9999
2	10	Appalachian Basin	Devonian	Oriskany Sandstone	30**	9999	9999	9.88^	25^	9999
3	14	Atlantic Coastal Plain	Cretaceous	Cape Fear	30**	0.2*	300*	16.88^	20^	0.12^
4	14	Atlantic Coastal Plain	Cretaceous	Lower Potomac Group	30**	0.2*	300*	16.88^	20^	0.12^
5	14	Atlantic Coastal Plain	Cretaceous	Tuscaloosa	30**	9999	300*	16.88^	20^	0.08^
6	21	Black Warrior Basin	Mississippian	Pottsville	10**	0.10*	20**	16.26^	15^	0.12^
7	22	Denver Basin	Cretaceous	Lyons Sandstone	20**	0.13**	38**	8.83^	30^	0.08^
8	31	Illinois Basin	Ordovician	St. Peter	30**	0.09**	300**	12.09^	20^	9999
9	36	Los Angeles Basin	Miocene	Repetto	16**	0.25*	200**	17.68^	40^	0.08^
10	37	Michigan basin	Ordovician-Cambrian	Mt. Simon	20**	0.09**	10**	12.09^	20^	0.12^
11	41	Palo Duro Basin	Paleozoic	Granite Wash	20**	0.15**	20**	14.06^	20^	9999
12	44	Permian Basin	Permian	Dean	15**	9999	11**	15.64^	20^	0.12^
13	44	Permian Basin	Permian	Queen	15**	9999	11**	15.64^	20^	0.12^
14	44	Permian Basin	Permian	San Andres	15**	9999	11**	15.64^	20^	0.12^
15	44	Permian Basin	Permian	Spraberry	15**	9999	11**	15.64^	20^	0.12^
16	44	Permian Basin	Permian	Wolfcamp	15**	9999	11**	15.64^	20^	0.12^
17	44	Permian Basin	Permian	Yates	15**	9999	11**	15.64^	20^	0.08^
18	45	Powder River Basin	Cretaceous	Fox Hills	30**	0.21*	50*	7.38^	30^	0.12^
19	54	San Juan Basin	Jurassic	Morrison	30**	0.23**	300**	8.95^	40^	9999
20	56	South Florida Basin	Cretaceous	Cedar Keys	20**	0.25*	20*	21.97^	25^	0.12^
21	58	U.S. Gulf Coast	Oligocene	Oligocene	30**	0.22**	200**	20.93^	35^	0.12^

22	61	U.S. Gulf Coast	Cretaceous	Woodbine	20**	9999	9999	20.93^	35^	9999
23	61	U.S. Gulf Coast	Cretaceous	Paluxy Sand	20**	9999	41**	20.93^	35^	0.12^
24	57	U.S. Gulf Coast	Eocene	Wilcox Group	20**	0.25**	115**	20.93^	35^	0.12^
25	69	Williston Basin	Carboniferous	Madison Group	17 **	0.10*	14**	14.22^	20^	9999

Table 6.4: GCCC Data input overview, summarizing data values and sources for Net to Gross Ratio (NG, %), Porosity (%), Permeability (mD), Surface Temperature (°C), Geothermal Gradient (°C/km) and Salinity (kg/L) data . Data sources: GCCC gridded data (9999), GCCC single value data (*), USGS single value data (**), other data sources (^)

6.3.3 MERGING USGS AND GCCC DATABASES

The USGS and GCCC databases were categorized and merged by a common formation group, or System, category. Because the USGS consolidated database has a total of 74 Systems, and the GCCC database has only 25 reservoirs, not all of the USGS Systems were merged with GCCC gridded reservoir data. Table 6.5 summarizes which GCCC reservoirs were merged with the corresponding USGS consolidated database. Also, since the USGS data extent is greater than the GCCC data extent, the USGS data extent is considered as the maximum System formation extent in the "*CO_2 Capacity, Injectivity, and Cost*" database.

As with the methods used to consolidate the USGS database, overlapping GCCC reservoirs' input data from different basins were consolidated to create three new reservoirs. These new reservoirs are the 1) Atlantic, which merges the GCCC's Tuscaloosa, Lower Potomac Group, and Cape Fear reservoirs; 2) Permian, which merges the GCCC's Yates, Queen, San Andres, Spraberry, Dean, and Wolfcamp reservoirs; and 3) Gulf of Mexico Cretaceous (USCret), which merges the GCCC's Woodbine and Paluxy reservoirs. The data per reservoir was consolidated by either summing the data values per reservoir (i.e., Storage Window Formation Thickness, and Net Sand Thickness), averaging the data (i.e., Depth to Formation), or generating a weighted average of the data values (i.e., Porosity and Permeability). With the consolidated reservoirs, the total number of GCCC reservoirs decreases from 25 to 17, as shown in Table 6.5.

Furthermore, in the 17 Systems where GCCC and USGS data overlap, the gridded GCCC data always supersedes USGS data. Figure 6.5 shows an example of a System where there is no merged GCCC data with USGS data, while figure 6.6 shows an example of the GCCC data superseding USGS data for the U.S. Gulf Coast Eocene System.

System ID	Basin	System	GCCC Reservoir Name
1	Alaska North Slope	Carboniferous	
2	Alaska North Slope	Cretaceous	
3	Anadarko and Southern Oklahoma Basins	Cambrian	Arbuckle Group
4	Anadarko and Southern Oklahoma Basins	Devonian	
5	Anadarko and Southern Oklahoma Basins	Mississippian	
6	Anadarko and Southern Oklahoma Basins	Permian	
7	Appalachian Basin	Ordovician-Cambrian	
8	Appalachian Basin	Lower Silurian	
9	Appalachian Basin	Upper Silurian	
10	Appalachian Basin	Devonian	Oriskany Sandstone
11	Arkoma Basin	Ordovician	
12	Arkoma Basin	Silurian - Devonian	
13	Arkoma Basin	Carboniferous	
14	Atlantic Coastal Plain	Cretaceous	Atlantic: Tuscaloosa, Lower Potomac Group, Cape Fear
15	Bend Arch and Fort Worth Basin	Ordovician - Mississippian	
16	Bend Arch and Fort Worth Basin	Carboniferous	
17	Bighorn Basin	Pennsylvanian	
18	Bighorn Basin	Permian	
19	Bighorn Basin	Triassic	
20	Bighorn Basin	Cretaceous	
21	Black Warrior Basin	Mississippian	Pottsville
22	Denver Basin	Cretaceous	Lyons Sandstone
23	Eastern Great Basin	Jurassic	
24	Eastern Mesozoic Rift Basins	Triassic	
25	Greater Green River Basin	Paleozoic	
26	Greater Green River Basin	Triassic-Jurassic	
27	Greater Green River Basin	Cretaceous	
28	Hanna, Laramie, and Shirley Basins	Paleozoic	
29	Hanna, Laramie, and Shirley Basins	Cretaceous	
30	Illinois Basin	Cambrian	
31	Illinois Basin	Ordovician	St. Peter
32	Illinois Basin	Devonian-Silurian	
33	Kandik Basin	Devonian	

System ID	Basin	System	GCCC Reservoir Name
34	Kandik Basin	Permian	
35	Kansas Basins	Paleozoic	
36	Los Angeles Basin	Miocene	Repetto
37	Michigan Basin	Ordovician-Cambrian	Mt. Simon
38	Michigan Basin	Silurian	
39	Michigan Basin	Devonian	
40	Palo Duro Basin	Paleozoic	Granite Wash
41	Palo Duro Basin	Permian	
42	Paradox Basin	Paleozoic	
43	Permian Basin	Paleozoic	
44	Permian Basin	Permian	Permian: Yates, Queen, San Andres, Spraberry, Dean, Wolfcamp
45	Powder River Basin	Pennsylvanian	
46	Powder River Basin	Triassic	
47	Powder River Basin	Jurassic	
48	Powder River Basin	Cretaceous	Fox Hills
49	Sacramento Basin	Cretaceous	
50	Sacramento Basin	Eocene	
51	San Joaquin Basin	Cretaceous	
52	San Joaquin Basin	Oligocene	
53	San Joaquin Basin	Miocene	
54	San Juan Basin	Jurassic	Morrison
55	San Juan Basin	Cretaceous	
56	South Florida Basin	Cretaceous	Cedar Keys
57	U.S. Gulf Coast	Eocene	Wilcox Group
58	U.S. Gulf Coast	Oligocene	Oligocene
59	U.S. Gulf Coast	Miocene	
60	U.S. Gulf Coast	Jurassic	
61	U.S. Gulf Coast	Cretaceous	USCret: Woodbine, Paluxy Sand
62	Uinta and Piceance Basins	Paleozoic	
63	Uinta and Piceance Basins	Cretaceous	
64	Uinta and Piceance Basins	Tertiary	
65	Ventura Basin	Oligocene	
66	Western Oregon-Washington Basins	Paleogene	
67	Williston Basin	Cambrian and Ordovician	
68	Williston Basin	Devonian	

System ID	Basin	System	GCCC Reservoir Name
69	Williston Basin	Carboniferous	Madison Group
70	Williston Basin	Jurassic	
71	Williston Basin	Cretaceous	
72	Wyoming-Idaho-Utah Thrust Belt	Paleozoic	
73	Wyoming-Idaho-Utah Thrust Belt	Triassic-Jurassic	
74	Wyoming-Idaho-Utah Thrust Belt	Cretaceous	

Table 6.5: Merged USGS and GCCC Data input summary table.

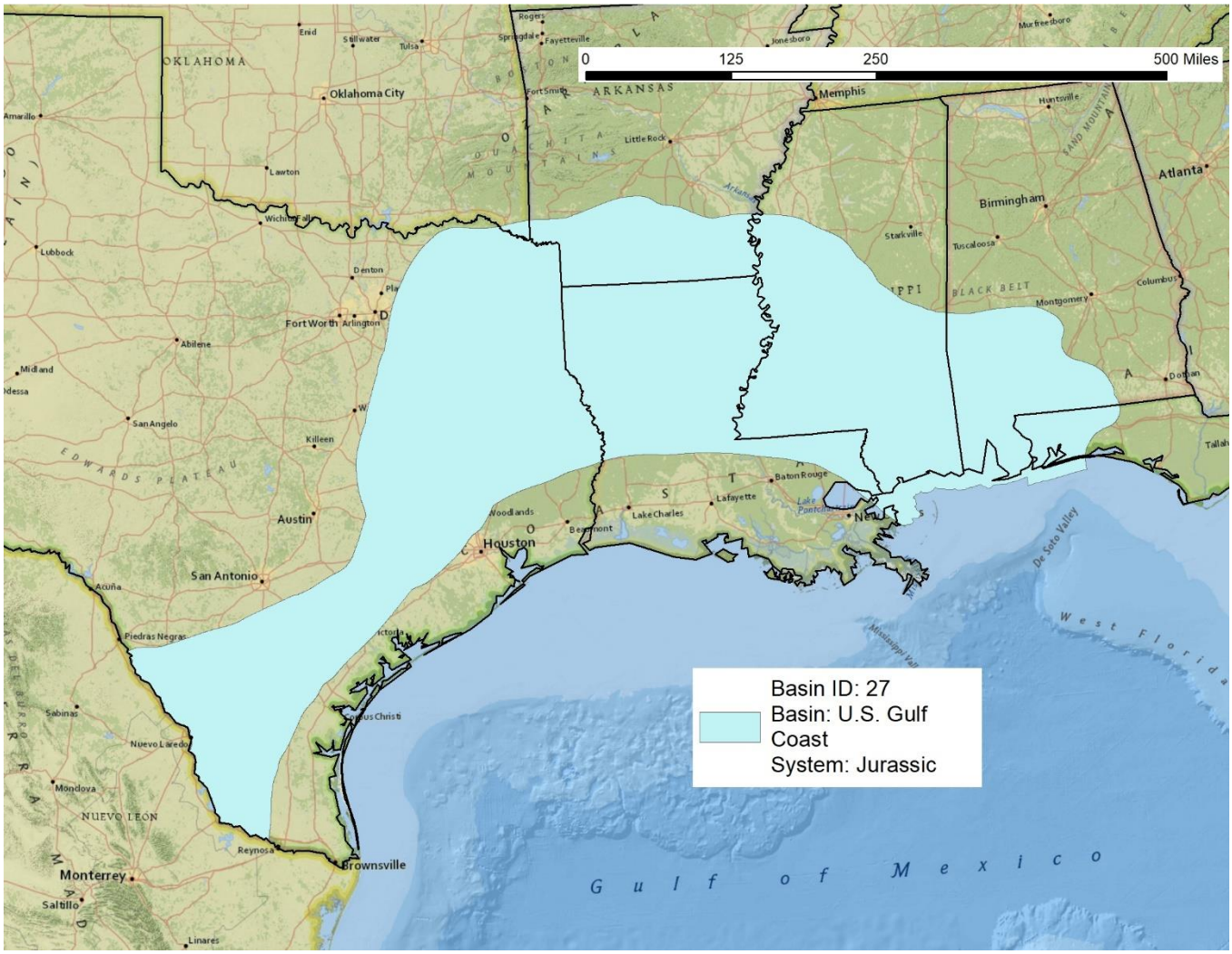

Figure 6.5: Jurassic System extent within the U.S. Gulf Coast Basin (ID 60). The system extent is defined by the USGS data extent. No GCCC data has been merged with the USGS data for this system.

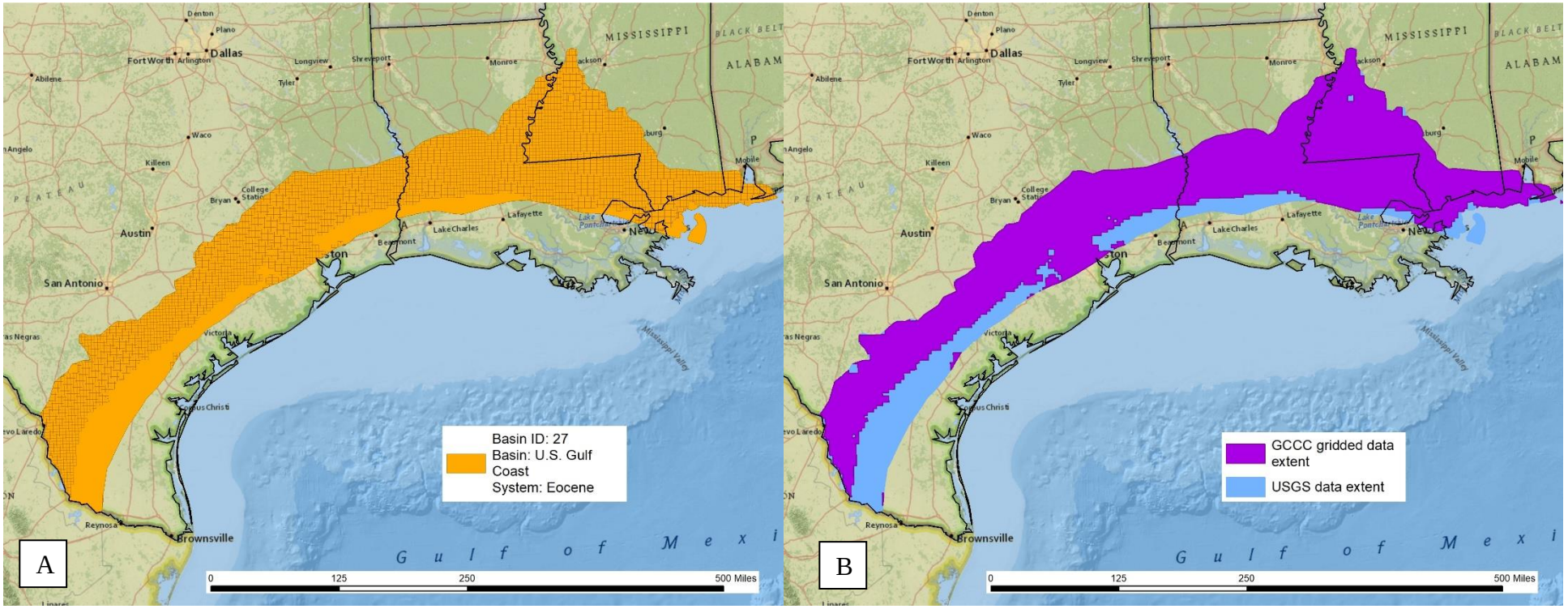

Figure 6.6: A) Eocene System extent within the U.S. Gulf Coast Basin (ID 57). The full data extent is defined by the USGS data extent, but most of the data has been superseded by GCCC data . The extent of the GCCC gridded data is better shown in B) in purple, while the remainder of the USGS data is shown in blue.

6.4 INPUT DATA QUALITY RANKING

In this section, a simple data quality ranking of the input data gathered to create the U.S. Wide Capacity, Injectivity, and Cost Analysis Database is introduced. The data quality ranking ranges from 3, which is the highest ranking, to 1, which is the lowest ranking. A higher ranking generally means that the data are more accurate. The input data considered for quality ranking includes the GCCC and USGS databases, as well as the supplementary data introduced in section 6.2. Note that the data quality ranking is not included in the database itself.

Ranking the data quality helps to quantify the potential error margin of the capacity, injectivity, and cost calculated results based on the accuracy of the input data. For example, the GCCC gridded data provides a higher resolution and data variation per area, which is considered to have a higher data accuracy. Thus, gridded data is considered to be the highest possible ranking. Table 6.6 below summarizes descriptions and error margins for all three data quality rankings.

Rank	Description	Input data source	Error	+/-
3	Diminished data: depth-dependent grid maps	Gridded GCCC data	0-25%	25%
2	Proxy info data: one average value per formation	All USGS data; GCCC single value data for porosity and permeability	25-50%	50%
1	Sparse data: poorly constrained average value	Basin-wide extent data: Geothermal gradient, Surface Temperature, and Salinity supplemental data	50-75%	75%

Table 6.6: Input data quality ranking description summary. A higher ranking indicates that the input data tends to be more accurate. 1 = lowest ranking, 3 = highest ranking.

6.5 DATA STRUCTURE

The resulting "*CO_2 Capacity, Injectivity, and Cost*" database contains three main spatial datasets: 1) "*Capacity Injectivity Cost Data",* 2) "*Highest Injectivity Analysis*", and 3) "*CO_2 Sedimentary Storage Window*" which will be further discussed in this section. Both datasets are saved within an ArcGIS geodatabase (.gdb) as feature classes and can only be accessed using the ArcGIS software. The spatial reference, quality, and general information for both spatial datasets are summarized in Table 6.7 below.

	Capacity Injectivity Cost Data	**Highest Injectivity Analysis**	**CO_2 Sedimentary Storage Window**
Geographic Coordinate System	GCS_North_American_1983		
Projected Coordinate System	USA_Contiguous_Lambert_Conformal_Conic		
Resolution	5km by 5 km for grid-like data. Varies for USGS-data		N/A
Number of Rows	47,997	54,060	N/A
Data file format	ArcGIS Feature Class		ArcGIS Feature Dataset
Type of Data	Polygon		

Table 6.7: "CO_2 Capacity, Injectivity, and Cost" database spatial references, data quality, data file formatting, among other data features.

6.5.1 CAPACITY/INJECTIVITY/COST & HIGHEST INJECTIVITY ANALYSIS DATA

Both the "*Capacity Injectivity Cost Data*" and the "*Highest Injectivity Analysis*" spatial data consist of the input data and output calculations described throughout Chapters 2 through 5. Both datasets result from the amalgamation of the GCCC and USGS databases, along with the supplementary data discussed in detail earlier in this chapter. Table 6.8 below summarizes the column descriptions for both datasets.

Field Name	Description	Units
Basin	Basin Name	none
System	System Name	none
GCCC_Reservoir_Name	Original reservoir name from GCCC data	none
Database_Key	original reservoir key from GCCC data	none
DF_m	Depth to Formation	m
SWFT_m	Storage Window Formation Thickness	m
MPD_m	Midpoint Depth	m
NetPorousTh_m	Net Porous Thickness	m
NG	Net to Gross Injectable interval	%
Porosity_per	Porosity	%
Permeability_mD	Permeability	mD
SurfTemp_C	Surface Temperature	C
GeothGrad_Ckm	Geothermal Gradient	C/km
ResTemp_C	Reservoir Temperature	C
Injectivity_mDm	Injectivity	mD-m
Wells	Number of Wells needed for 1 Mtpa per project	wells
AllowPInc_MPa	Allowable Pressure Increase	MPa
Salinity_kgL	Reservoir Salinity	kg/L
TotalComp_1MPa	Total Compressibility	MPa^{-1}
CO2Density_kgm3	CO_2 Density	kg/m^3
CapacityArea_Mtkm2	CO2 Capacity per Area	Mt/km^2
Capacity_Mt	CO_2 Storage Capacity	Mt
WellSpacing_km	Spacing between wells within one project	km
AreaPer20MtProject_km2	Area of a Project with a 20 yr lifetime injecting at 1 Mtpa	km
GCCC	Keep track of data source	1 = GCCC data, 0 = USGS data
TotalCost20yr1Mtproject_USD	Total Cost of a CCS Project with a 20 yr lifetime injecting at 1 Mtpa	$MM USD
TotalStorageCost_USDperTon	Total Storage Costs in $ per Ton of CO_2	$USD per Ton of CO2

Table 6.8: Summarized Field/Column names and descriptions for both the "*Capacity Injectivity Cost Data*" and "*Highest Injectivity Analysis*" spatial data. ArcGIS categorizes columns in a table as Fields. Mt = million metric tons Mtpa = Million metric tons per annum (per year).

The "*Highest Injectivity Analysis*" spatial dataset takes the "*Capacity Injectivity Cost Data*" dataset and chooses the Systems with the best injectivity to properly view and analyze the area-based storage costs. In some areas within the "*Capacity Injectivity Cost Data*" , the spatial data has overlapping features where two or more Systems exist within the same area extent (i.e., the U.S. Gulf Coast Basin's Systems). Seen on a 2D map, the results shown from areas where data overlaps only show the top-most System. The "*Highest Injectivity Analysis*" dataset is the result of comparing injectivity results between overlapping data found in the "*Capacity Injectivity Cost Data*" dataset and choosing the highest injectivity value between them. Overlapping data with lower injectivity are discarded from the "*Highest Injectivity Analysis*" database but are kept within the "*Capacity Injectivity Cost Data*" dataset. Understanding how to place wells and projects for areas that share overlapping Systems is beyond the scope of the current study.

6.5.2 CO_2 SEDIMENTARY STORAGE WINDOW

The "*CO_2 Sedimentary Storage Window*" dataset contains two feature classes, 3a) "*Storage Window Potential*" and 3b) "*No Storage Window Potential*"*".* The two feature classes are the result of the data and methodologies described in detail in Chapter 2. The "*CO_2 Sedimentary Storage Window*" spatial data assigns a ranking from 1 to 4, with 1 being the lowest CO_2 storage potential. The ranking is based on the total sedimentary thickness within the storage window. As for the "*No Storage Window Potential"* spatial data, it comprises the no storage criteria described in section 2.4.

Chapter 7: Results

7.1 INTRODUCTION

This chapter contains a compilation of maps and figures from the methodologies described throughout Chapters 2 through 5, as well as the "*CO_2 Capacity, Injectivity, and Cost*" database created for this thesis, described in Chapter 6. The results from each chapter are described in detail below.

7.2 SEDIMENTARY CO_2 STORAGE WINDOW POTENTIAL

The results from the sedimentary CO_2 storage window (SSW) concept introduced in Chapter 2 are displayed in Figure 7.1 as potential for CO_2 storage throughout the U.S., varying from lowest to highest thickness using a numeric ranking system. The ranking system begins at 0, indicating areas of no storage window potential, to 4, the highest storage window thickness in an area. Table 7.1 below summarizes the SSW potential ranking and its corresponding range of sedimentary thickness available within the storage window.

Complementary to the SSW is the top window concept, which is a heavily influential boundary condition for the calculation and creation of pressure-based capacity and injectivity, which in turn also influences storage and project costs. Figure 7.2 shows the top window boundary condition, renamed as the Depth to Top Storage Window for Figure 7.2. The data has not been included in the "*CO_2 Capacity, Injectivity, and Cost*" database.

SSW Potential Ranking	SSW Potential Description	Sedimentary Thickness range (m)
0	No Storage Window Potential	0
1	Lowest	0 - 1000
2	Low-Medium	1001 - 2000
3	Medium-High	2001 -3000
4	Highest	> 3000

Table 7.1: Sedimentary CO2 Storage Window (SSW) Potential ranking used for Figure 7.1.

7.3 PRESSURE-BASED STORAGE CAPACITY

The results from the pressure-based storage capacity introduced in Chapter 3 are displayed in Figure 7.3 showing the cumulative storage capacity per unit area for all 74 Systems found within the "*Capacity Injectivity Cost Data*" spatial dataset. This dataset contains overlapping Systems that contain different input data and results. In order to display the capacity per unit area results from all Systems in the same map, the choice was made to sum all overlapping Systems. The resulting cumulative storage capacity map displays a range of capacity per given area, with the lowest being around 50,000 tons, or 0.05 million tons of CO_2 per 1 km^2 for various basins across the U.S., and the highest being around 2.2 million tons of CO_2 per 1 km^2 in a small section of the U.S. Gulf Coast's Miocene System.

7.4 INJECTIVITY

The results from the concept of injectivity introduced in Chapter 4 are displayed in Figure 7.4 as an injectivity rank and a range of wells needed to inject 1 million tons of CO_2

per year (Mtpa) per project based on the highest injectivity Systems in a given area. The injectivity ranking ranges between lowest, where the lowest injectivity but highest number of wells are found, to highest, where the inverse is true. The number of wells ranges from 1 to 19 per project (P10 to P90), with 16 wells being the average. The results suggest that the U.S. Gulf Coast Systems have the best injectivity; whereas the Appalachian and Bend Arch/Fort Worth Basin Systems trend towards low injectivity values. Table 7.2 summarizes the injectivity ranking, description, injectivity value ranges, and number of wells per rank. The results displayed in Figure 7.4 originate from the "*Highest Injectivity Analysis*" spatial dataset, which means that not all results from each System are represented in this map.

Rank	Description	Injectivity (mD-m)	No. of Wells
1	Lowest	0 to 500	> 20
2	Low Medium	500 to 1500	7 to 20
3	Medium	1500 – 5000	2 to 6
4	Medium High	5001 – 10000	2
5	Highest	> 10000	1

Table 7.2: Injectivity Ranking utilized in Figure 7.4. The number of wells represents the total amount of wells needed to inject 1 Mtpa within each CCS project.

7.5 CCS PROJECT STORAGE COST

The results from the storage and CCS project cost methodology introduced in Chapter 5 are displayed in Figure 7.5 and Figure 7.6, showing a range of storage costs per ton of CO_2 and a range of storage costs for a potential 20 Mt CCS project with a 20-year lifespan, respectively. Note again that the CCS project costs only consider storage-related

costs and do not consider capture nor potential transportation costs. Figure 7.5 presents the five price ranges that reflect the current average cost range of storing CO_2 per ton (i.e., $5 to $30 USD) (IEA, 2022c). Table 7.3 below summarizes the statistics for all of the resulting data costs.

Statistical Variable	Storage Costs ($ USD per ton CO2)	Total Project Storage Costs ($ MM USD)
Average	$ 30.70	$ 613.80
P10	$ 4.70	$ 94.27
P50	$ 7.30	$ 146.90
P90	$ 51.70	$1,033.60

Table 7.3: Storage costs and total project storage costs statistical summary

The data suggest that the least expensive areas for CO_2 storage are the onshore Gulf of Mexico Basin, the West Coast (San Joaquin, Sacramento, Ventura, and western Oregon-Washington Basins) and the Permian Basin, and the least expensive is the Gulf of Mexico Miocene System at $4.00 USD/ton of CO_2 (note that the offshore Gulf of Mexico Basin was excluded from the current study). It is not surprising that the same areas where storage costs are lowest having the lowest total costs per project, with the cheapest costing around $80 MM USD for a project that can take up to 20 Mt in 20 years. Table 7.4 summarizes shows the 10 least expensive Systems for storage and project costs. The top 1 through 8 Systems result from single-average values (Table 7.4a) and 9 and 10 originate from a range of values (gridded data), of which statistics can be provided (Table 7.4b). To reduce the effect of outliers when calculating the average value per System, only the results from data

stemming from 1.5 m net porous thickness and greater are considered. Tables A1 and A2 in Appendix A contain the remaining cost data.

It is important to note that the results displayed in Figures 7.5 and 7.6 originate from the "*Highest Injectivity Analysis*" spatial dataset, which means that not all results from each Systems are represented in this map.

	Basin	System	Storage Costs ($ USD per ton CO2)	Total Project Storage Costs ($ MM USD)
1	U.S. Gulf Coast	Miocene	4.00	79.09
2	San Joaquin Basin	Miocene	4.07	81.46
3	Sacramento Basin	Cretaceous	4.17	83.36
4	San Joaquin Basin	Cretaceous	4.17	83.39
5	Western Oregon-Washington Basins	Washington Basins Paleogene	4.23	84.56
6	San Joaquin Basin	Oligocene	4.24	84.83
7	Ventura Basin	Oligocene	4.36	87.22
8	Permian Basin	Paleozoic	4.62	92.43

Table 7.4a: Storage and CCS project storage costs for the top 8 least expensive Systems. Note that the top 8 results come from a single-average value per System, and so the cost results are also a single value representing the entire extent of the System.

ID	Basin	System	Storage Costs ($ USD per ton CO2)						Total Project Storage Costs ($ MM USD)					
			mean	min	P10	P50	P90	max	mean	min	P10	P50	P90	max
9	U.S. Gulf Coast	Oligocene	5.74	4.15	4.42	4.65	5.28	209.68	114.81	83.09	88.41	93.03	105.5	4193
10	U.S. Gulf Coast	Eocene	6.28	4.13	4.41	4.71	5.29	213.44	125.75	82.52	88.2	94.23	105.7	4268

Table 7.4b: Storage and CCS project storage costs for the top 9 and 10 least expensive Systems. Note that these two Systems contain multiple values (gridded data) throughout the extent of the System.

In areas within the storage window but with limited availability of geologic data, the costs resulted in $52.40 per ton of CO2. The results are based on the 90th percentile (P90) of the storage costs per project ($51.70) and the P90 of the area per project (9,300 km^2). The results for the storage cost analysis have been combined with the storage costs per ton spatial distribution results mentioned earlier in this section and are displayed in Figure 7.7.

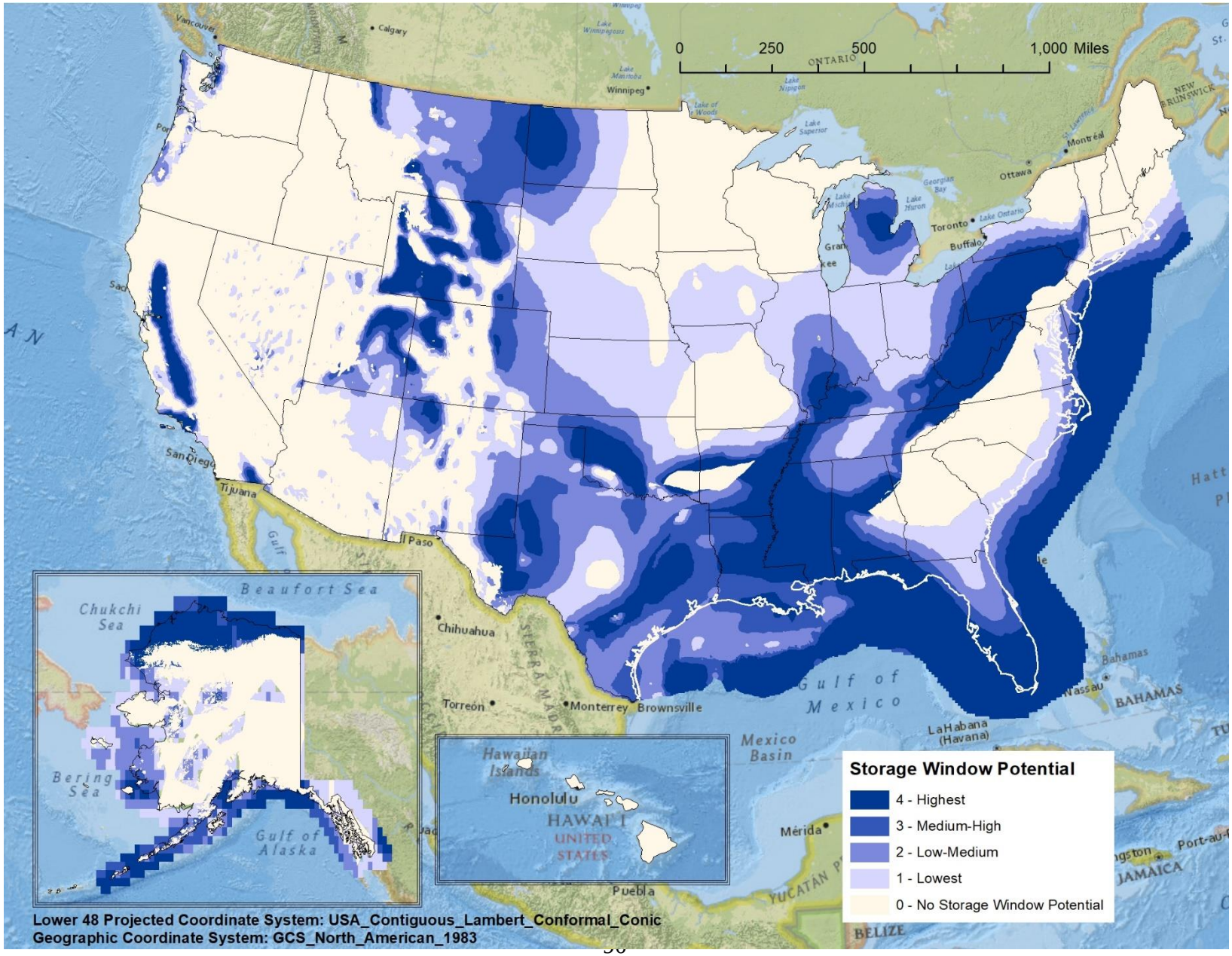

Figure 7.1: U.S.-Wide CO2 Sedimentary Storage Window map, displayed as increasing storage window thickness (1 = lowest, 4 = highest, white = no storage potential). Data taken from the "CO2 Sedimentary Storage Window" spatial dataset.

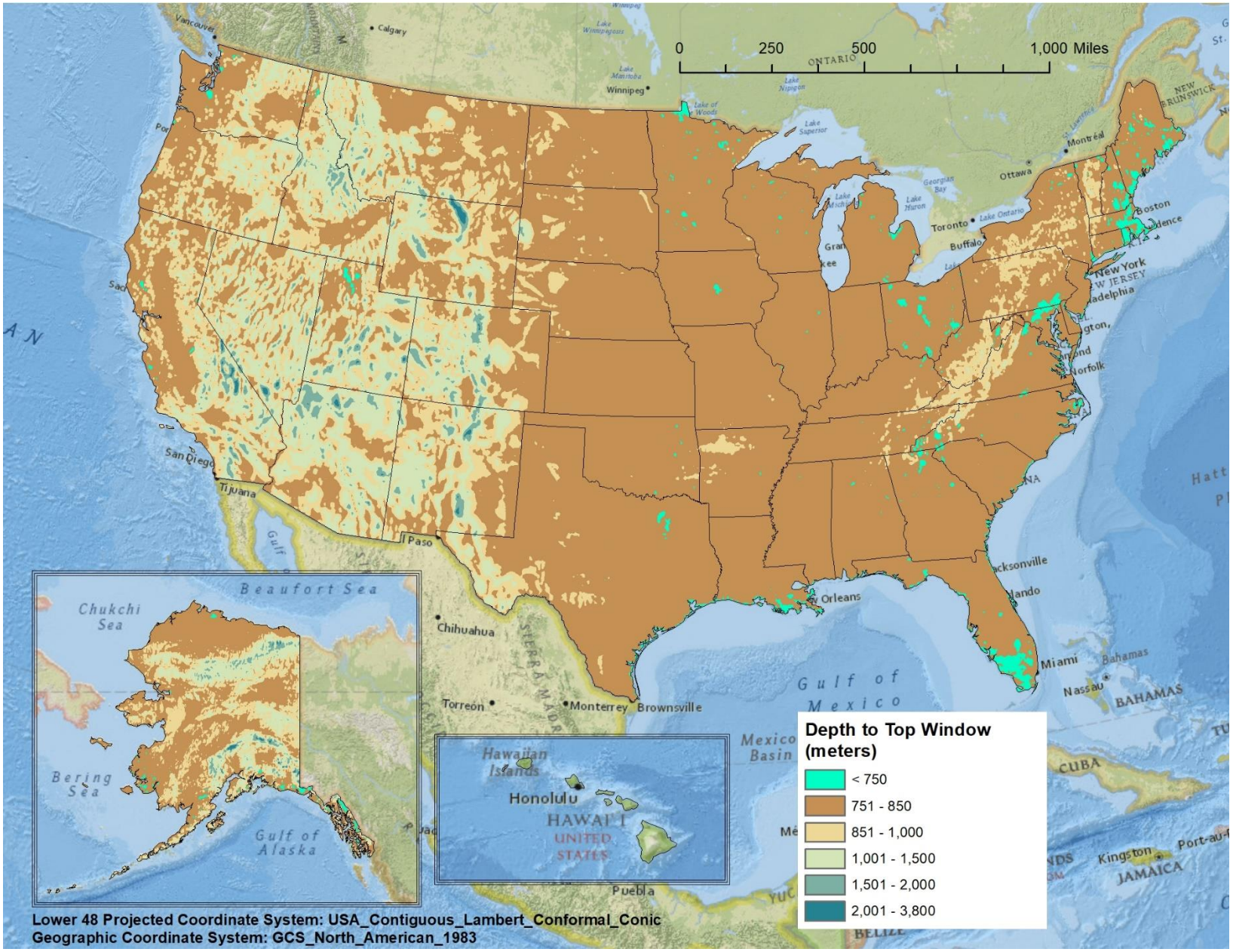

Figure 7.2: Depth to Top of Storage Window, in meters. Original data from De Graaf et al. (2017) not included in this thesis.

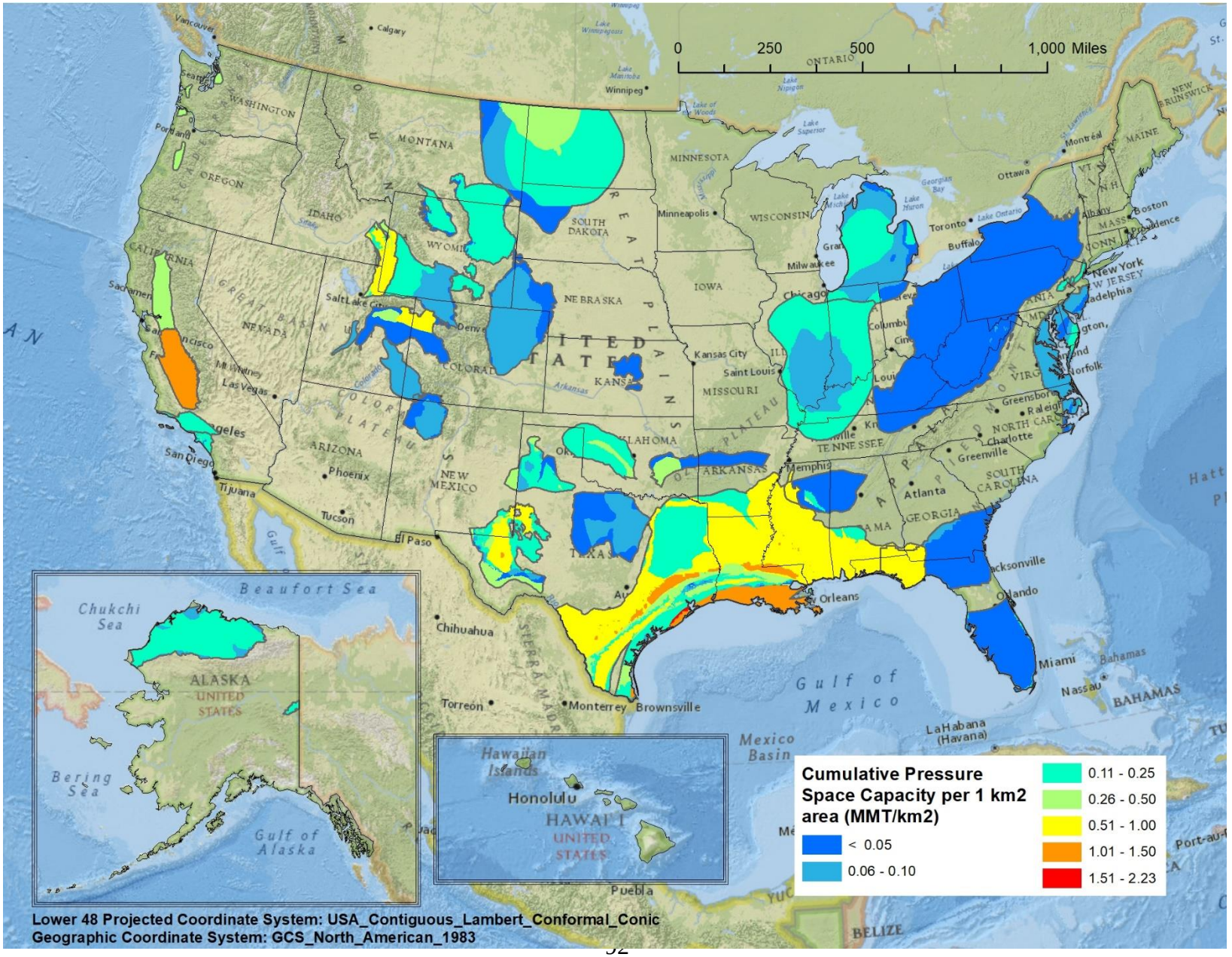

Figure 7.3: Cumulative Pressure-based Storage Capacity (Mt) per 1 km2 area. A higher capacity per area value means there is a higher capacity storage potential in a given area. Data taken from the "Capacity Injectivity Cost Data" spatial dataset.

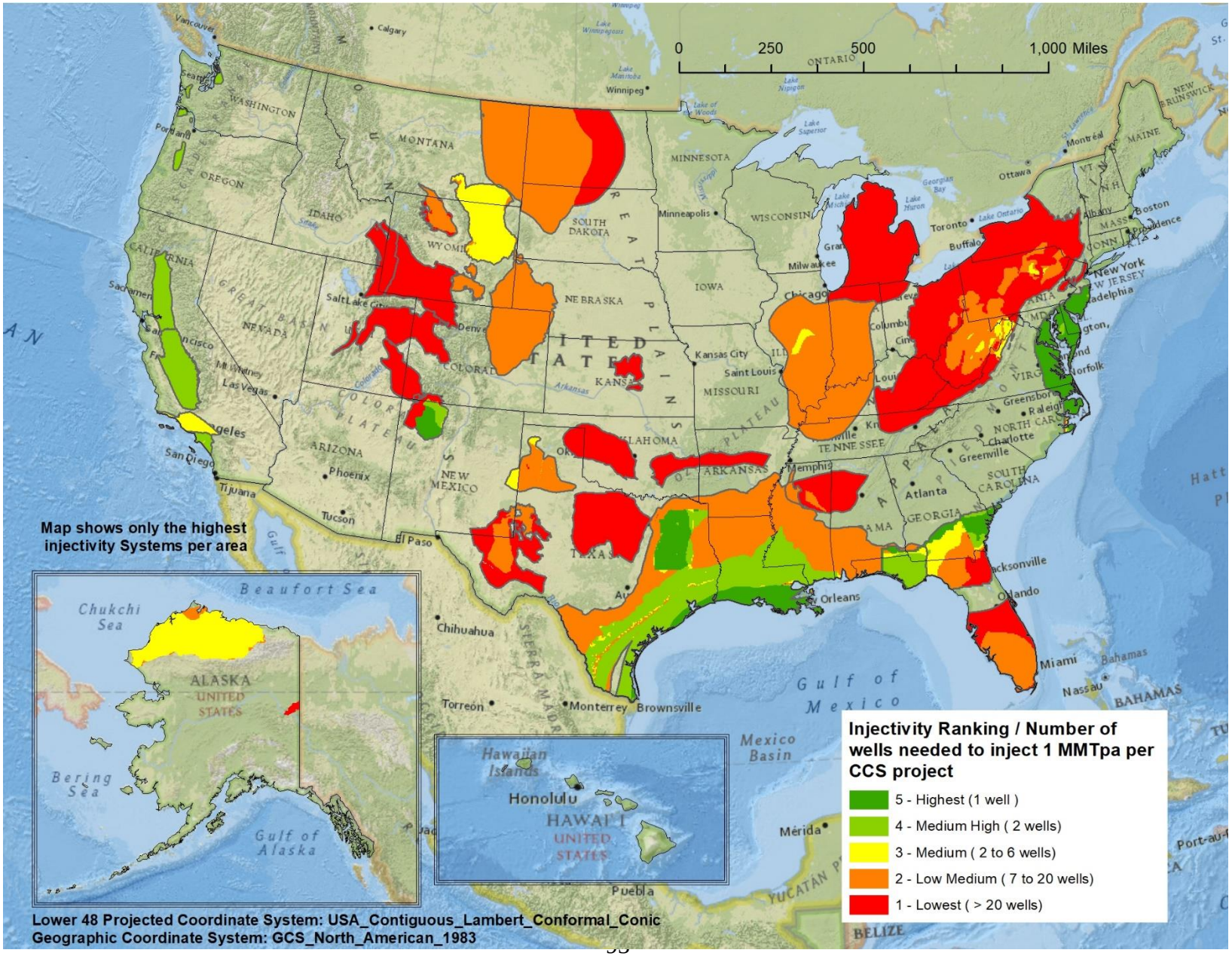

Figure 7.4: Injectivity Ranking (Low to High) of the highest injectivity systems per displayed area. Each injectivity ranking has a contingent number of wells needed to inject at a rate of 1 Mtpa per project. Data taken from the "Highest Injectivity Analysis" spatial database.

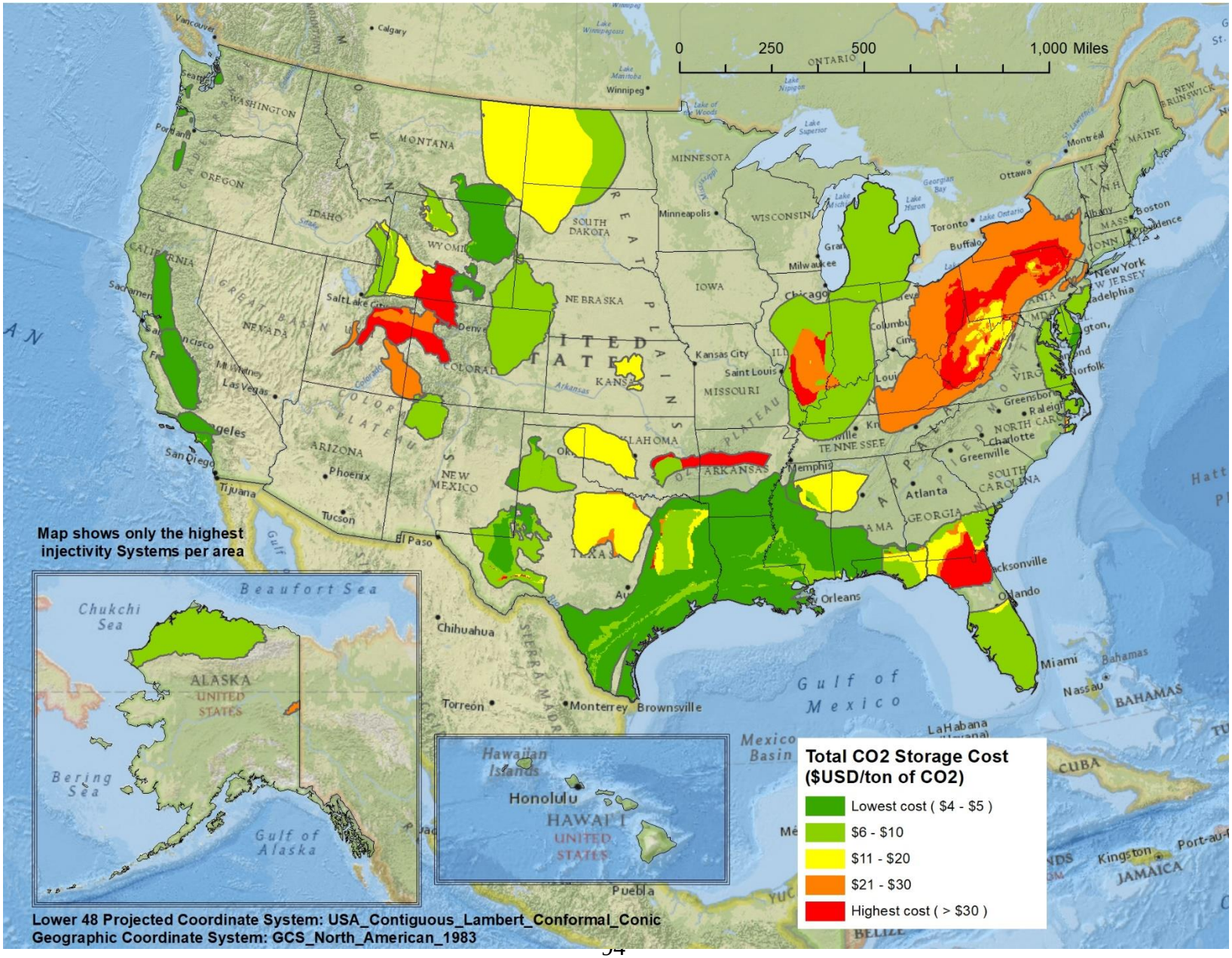

Figure 7.5: Storage Costs ($ USD) per ton of CO_2. Data taken from the "Highest Injectivity Analysis" spatial database.

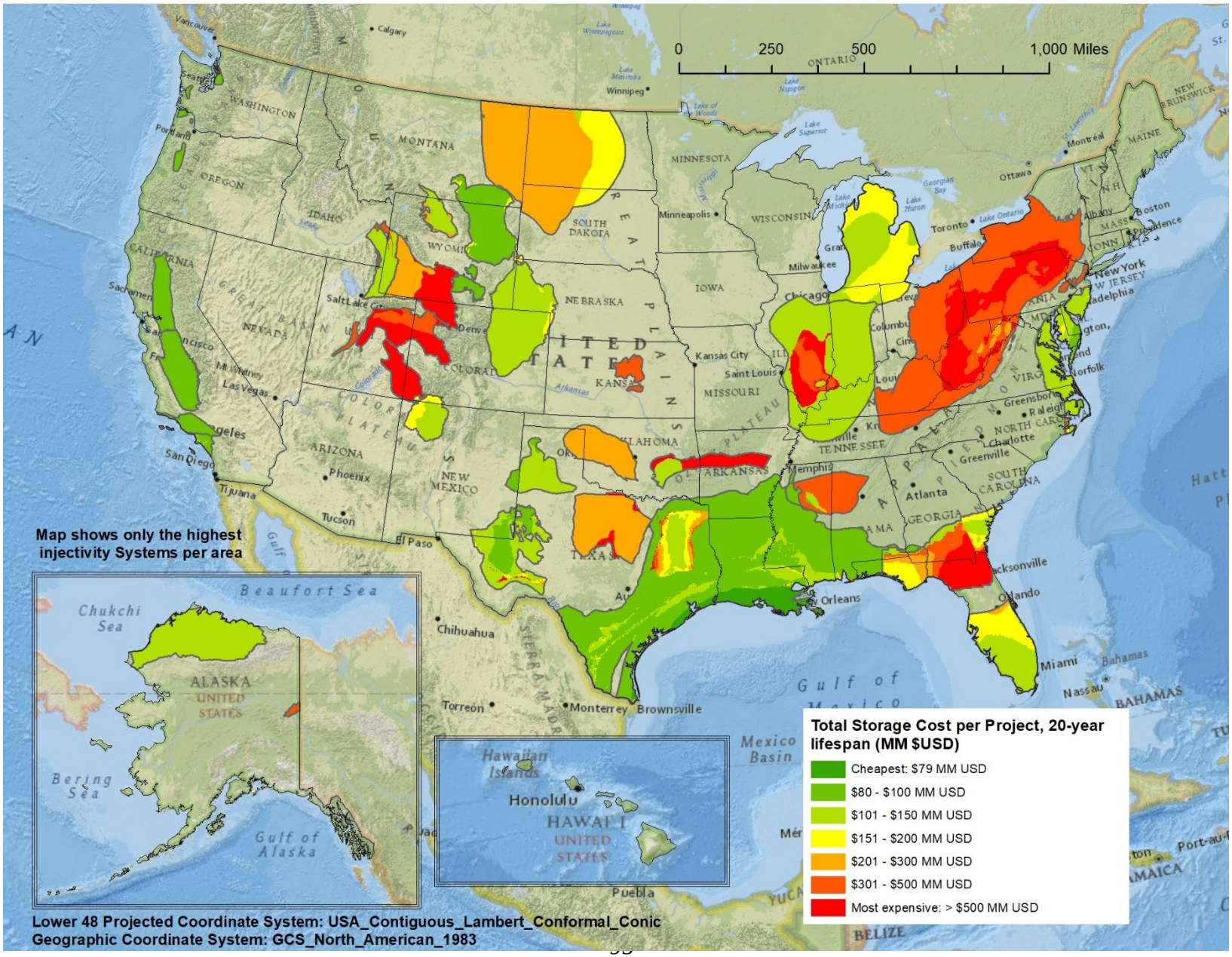

Figure 7.6: Total Storage Cost ($ MM USD) per CCS project over a 20-year lifespan. Data taken from the "Highest Injectivity Analysis" spatial database.

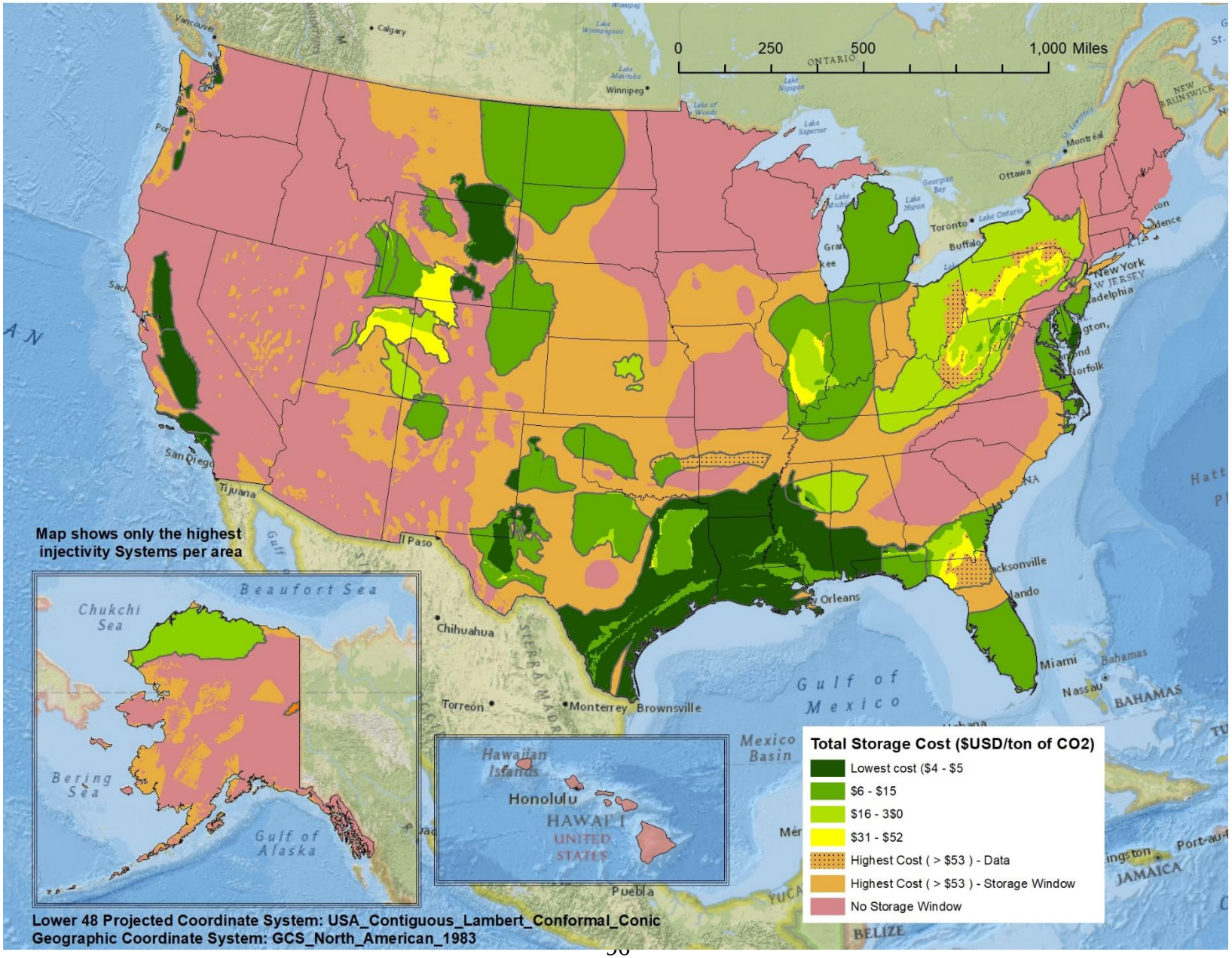

Figure 7.7: Storage Costs ($ USD) per ton of CO_2 including costs calculated for remaining storage window (non-dotted areas in orange) and no storage areas in red. Dotted highest storage costs are results from database. The areas within the storage window that have limited to no data but could be explored for storage in the future. Data taken from the "Highest Injectivity Analysis" spatial database.

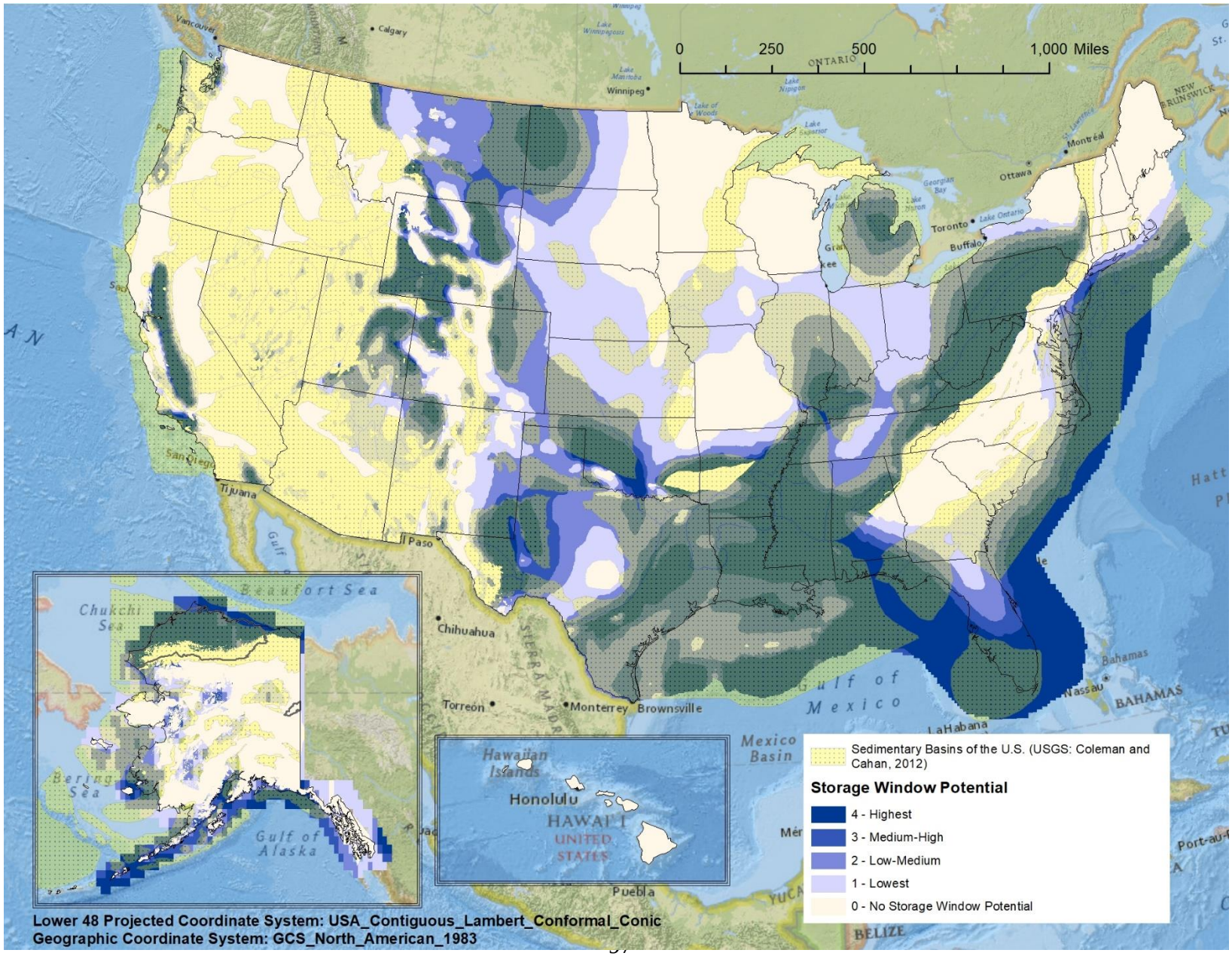

Figure 7.8: U.S.-Wide CO2 Sedimentary Storage Window map with overlaying Sedimentary Basins of the U.S. data from USGS (Coleman and Cahan, 2012).

Chapter 8: Discussion

8.1 INTRODUCTION

This chapter focuses on a general discussion of the results shown in Chapter 7, as well as the assumptions and limitations involved in the creation and analysis of the resulting capacity, injectivity, and storage costs data.

8.2 SEDIMENTARY CO_2 STORAGE WINDOW POTENTIAL

Figure 7.8 shows that, for the sedimentary CO_2 storage window (SSW) potential map, the areas where there is the highest storage thickness are located within major known U.S. sedimentary basins. This general insight provides a general reassurance that the SSW potential map is heading in the right direction, as the thickest layers of sedimentary rock are found within sedimentary basins. Sedimentary basins are areas where the most data have been collected as a result of hydrocarbon activities and compiled in previous studies.

The most exciting results from mapping the SSW are the identification of both new potential areas outside U.S. sedimentary basins that had not been previously considered for either CO_2 storage nor exploration, as well as the areas throughout the U.S where there is no possible storage potential. States like New Mexico, Kansas and Nebraska, to name a few, show low to low-medium storage potential, whereas most of the western states and a big chunk of Alaska show areas of no storage potential. Consequently, the identification of storage potential fills in a much-needed research gap for nationwide CO_2 storage potential.

The knowledge and identification of both new and no potential storage areas can lead to reducing the cost of CCS project's infrastructure and development and help accelerate the progress towards the net zero GHG and CDR goals. Although the new potential areas have generally lower storage potential compared to other more favorable

areas, the lower potential areas can act as smaller, more localized, and potentially cheaper CO_2 storage alternative (non-dotted, orange areas in Figure 7.8). Traditionally, CCS storage cost models assume that CO_2 point source emissions from facilities such as cement and energy plants are transported, usually through a pipeline, to the large geologic storage sinks (i.e., Middleton et al 2022). However, the cost of building new pipeline infrastructure is costly. Smith (2021) recognizes that the cost of a pipeline depends on distance to the source, as well as the amount of CO_2 being transported. Smith (2021) proposes 0.5 MM USD per mile of pipeline constructed to transport approximately 1 Mtpa of CO_2, with the cost increasing to around 1.25 MM USD per mile to transport 10 Mtpa of CO_2. Depending on the distance and amount of emissions that need to be transported, it is possible that storing CO_2 closer to the source, in less traditional sinks is cheaper than building the infrastructure to transport farther to higher quality sinks, which in turn lowers the cost of development of CCS projects.

8.3 STORAGE COSTS

One of the biggest contributions of this thesis is the implementation of the extent of pressure-based storage cost distributions paired with CCS projects throughout the U.S. By incorporating pressure space-based costs into the analysis, storage costs results offer a more realistic picture of the costs that go into developing a CCS project while at the same time considering pressure limitations and mitigating overpressure risks. This is important progress that can clarify overlapping interests between investors and regulators to make better, informed decisions about the development of CCS, particularly on a large-scale.

Providing improved regional storage project distribution results could benefit other CCS-related models such as pipeline infrastructure and placement models, by reducing storage uncertainty. The storage available, distance between the storage site and emission

sources, and the amount of CO_2 transported, are important variables for modeling pipeline locations, distance, and total costs, with models varying widely due to reservoir geology assumptions and uncertainty (McCoy and Rubin, 2005, Smith, 2021). Pipeline models could incorporate data such as the data presented here to reduce their storage uncertainty and provide more accurate transportation costs from their pipeline models.

Even capture technology, such as direct air capture (DAC) and biomass carbon removal and storage (BiCRS) could benefit from the optimization of storage costs and make both more economically feasible option in certain areas of the U.S. By far the most expensive portion of the development of CCS lies within the CO_2 capture costs, with DAC being the most expensive type of CO_2 capture ranging between $140 to $350 per ton of CO_2 captured (IEA, 2021). Lower storage costs can increase the DAC budget to either build larger DAC plants or operate an existing plant for a longer timeframe. Overall, lower storage costs could be a game-changer for both technologies, which could only benefit the overarching carbon dioxide removal goals set by the Biden Administration and help mitigate climate change.

8.4 LIMITATIONS

The following section discusses the limitations of the dataset presented in this thesis. The section is broken down into three parts, which include data, geologic, and data analysis limitations. The limitations on data focus on the quality of the data, while the geologic limitations focus on the presence and effect of complex geologic systems on pressure buildup. Finally, the limitations of the approach taken to analyze the dataset presented are discussed.

8.4.1 DATA LIMITATIONS

One of the biggest limitations regarding the accuracy of the cost estimates presented in this thesis is the use of poorly constrained average values based on sparse data to calculate pressure-based capacity and injectivity. Section 6.4 expands on the data quality for the types of data inputs used in this scope of work, of which the poorly constrained average values ranked the lowest (rank = 1). The most poorly constrained average values include: the net to gross (N:G) and distribution of porosity and permeability of the injection interval, salinity values, depth to injection intervals from USGS, and the geothermal gradient values. The range of error for these values dramatically increases the range of error for both capacity and injectivity calculations.

Another major limitation is the upscaling of the USGS data from their original categorization of geologic reservoirs of storage assessment units to Systems, the category introduced in this thesis. Although there was careful consideration of how the data was merged, the fact is that simplifying already averaged values probably decreased the data quality of the USGS data. However, simplifying the USGS data helped merge the data with GCCC database.

8.4.2 GEOLOGIC LIMITATIONS

This analysis is based on an extensional stress regime, which is appropriate for most of the U.S., including the major potential storage basins. For basins in compressional and strike-slip regimes, such as the west coast and Alaska, the calculation needs to be adjusted and would result in a different estimate of storage capacity.

This analysis also assumes that each project employs enough wells to access all of the pressure space within the calculated project area. That is, it assumes that each project area contains fewer isolated pressure compartments than wells. By and large, that seems a

reasonable starting point, but heavy faulting or complex, low net to gross depositional systems could create small compartments and potentially break this assumption (e.g., Figure 8.1). If that were the case, a given project would need either more wells or more area (if it focused only on compartments of a given size and neglected the smaller ones). Consideration of geologic complex structures could thus provide more accurate storage costs.

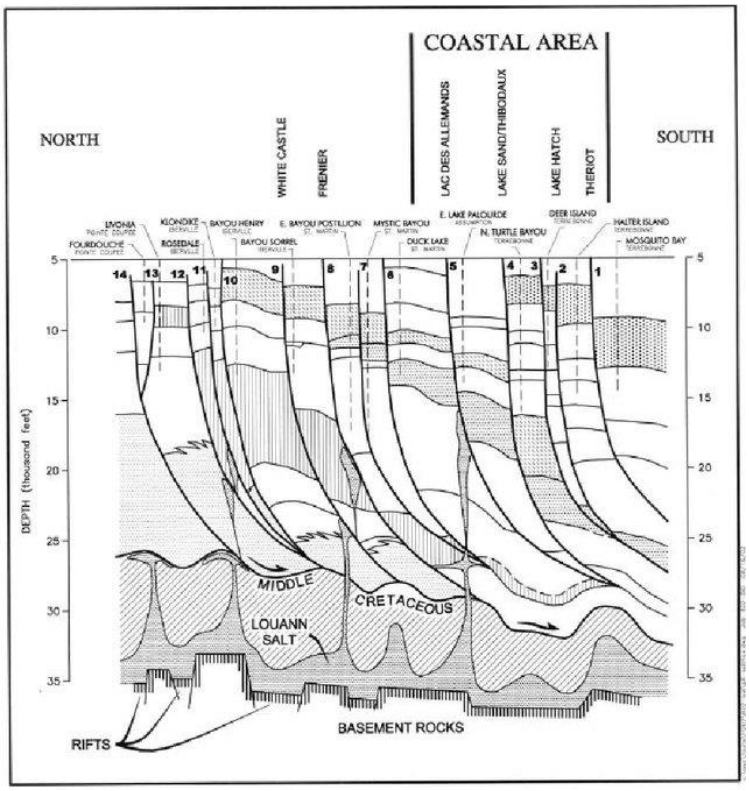

Figure 8.1: Geologic cross-section of coastal Louisiana, showing fault compartmentalization (Taken from Adams, 1997).

Furthermore, an increase in pressure in the subsurface caused by fluid injection can induce seismicity in areas where faulting exists. Fluid injection has been linked to induced seismicity in various contexts, including wastewater disposal (Ellsworth, 2013) and a few

documented cases in existing CCS projects (Kaven et al. 2015, Verdon et al. 2013). The additional pressure increases in the subsurface can alter the rock stress fields and stresses along faults, potentially reactivating them (Vilarrasa et al. 2019). Historic areas prone to induced seismicity have been identified to exist mainly in basins found along the west coast and the Anadarko basin in Oklahoma (Figure 8.2). Increasing injection may reveal new risks in other basins.

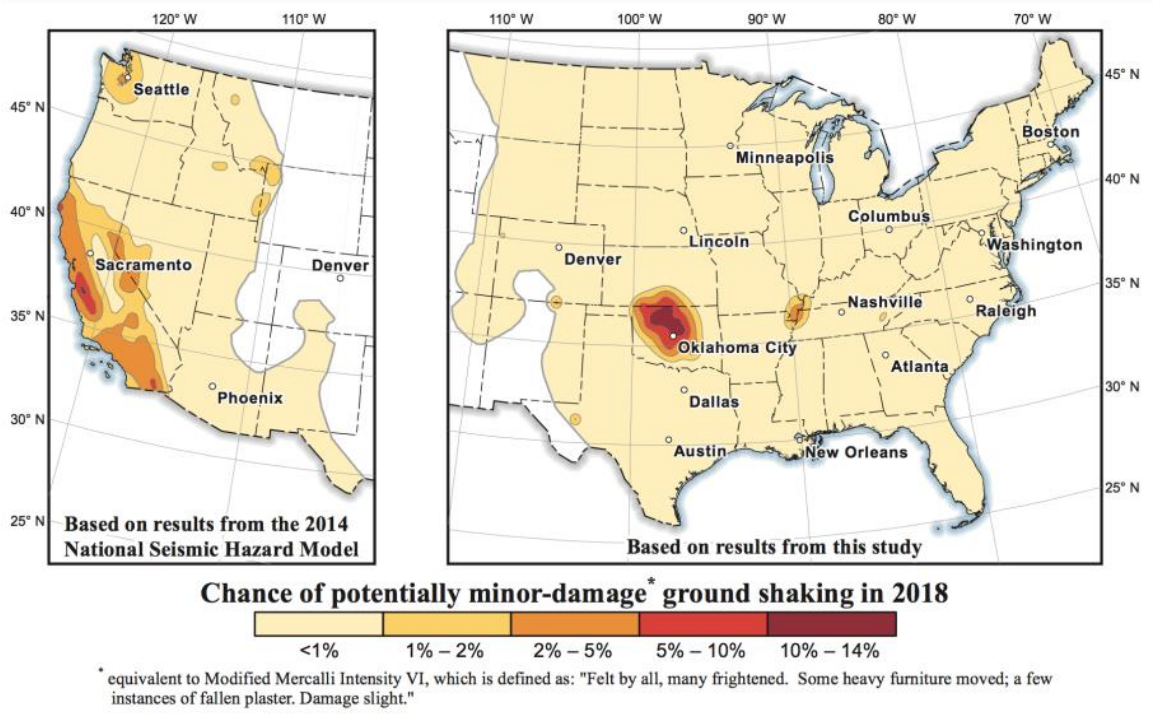

Figure 8.2: Chance of potentially minor damage ground shaking in 2018 from induced and natural earthquakes, one-year probabilistic seismic hazard (USGS, 2018)

As a precaution to mitigate the risk of induced seismicity, the pressure increase considered for pressure-based CO_2 storage capacity calculations reaches 90% of the calculated Eaton's fracture pressure, as detailed in section 3.3.8 and shown in eq. 3.10. However, even with a 90% reduction of the fracture pressure, the need to mitigate risk of

induced seismicity from fluid injection might limit the allowable pressure increase even further, which in turn decreases storage capacity calculations. Thus, further consideration of induced seismicity risk for areas prone to it should be included in future iterations of this work.

Lastly, the allowable pressure increase calculations are based on an average value of Poisson's ratio in sandstones, which is reasonable for a regional assessment dominated by clastics. However, accurate assessment of capacity in carbonate reservoirs would require slightly different Poisson's ratio values, which would slightly change the allowable pressure increase within a rock unit.

The errors generated by the approximations detailed here are generally likely to be small next to the errors resulting from the simplified input data.

8.4.3 RESULTS LIMITATIONS

The results for the CCS project storage costs are limited to only the Systems with the highest injectivity and forego the data of overlapping Systems. Consequently, in areas where overlapping Systems exist, there is more storage that can be realistically assessed within the same area. This is due to the challenge of completing a spatial analysis for the area of a CCS project when there are two or more overlapping Systems. Determining how project areas could interfere in the surface if the projects inject in different Systems is outside of the scope of this work. The SimCCS cost simulation tool does have the capability of analyzing stacked reservoirs (Ellet et al. 2017).

Additionally, results are limited to a constant capacity and injection rate for all CCS projects and forego a spatial distribution of neighboring smaller and/or larger CCS projects. For example, the current data analyzes area per project based on a constant capacity of 20

Mt per project. The capability to easily change the total capacity requirements of a project and thus changing the area per project would optimize and enhance storage costs.

Other factors that could increase capacity potential that were not included in this study include 1) dissolution as a secondary trapping mechanism and 2) brine extraction for pressure management. However, both factors have their own caveats, and need further consideration before aggregating them to the current database methodology. The pressure-based capacity calculations fail to consider dissolution as a secondary trapping mechanism. For example, the CO_2 can dissolve into the brine found within the porous media in a reservoir, decreasing the concentration of CO_2, which results in a reduction of the pressure exerted by the remaining CO_2 volume. Secondary trapping mechanisms can potentially improve CO_2 storage potential (Abba, 2019) but it is difficult to estimate by how much, even in previous CO_2 injection studies that included reservoir characterization has been done (Cranfield, Lu et al. 2013). The second factor, brine extraction, is a proven mature technology used to manage increasing pore space pressure from fluid injection into the subsurface. Extracting the brine from the subsurface theoretically increases the CO_2 capacity potential. However, the disposal of the brine produced from CCS is expensive, to the point where CCS infrastructure models show that it is more cost effective to move to a better storage spot than to implement brine extraction (Anderson and Jahediesfanjani, 2020).

Chapter 9: Conclusions and Future Work

9.1 CONCLUSION

In order to limit the detrimental impact of CO_2 emissions towards global warming, the U.S. and the Biden Administration set a net zero GHG goal by 2050 assisted by a carbon dioxide removal (CDR) goal of 1 Gtpa from the atmosphere. Carbon Capture and Storage (CCS) technology will be critical to reaching this goal. However, the current and planned CCS infrastructure is not nearly enough to reach the 1 Gtpa CDR goal in a timely manner, and thus large-scale development of CCS needs to be deployed as quickly as possible. The challenge with large-scale deployment is that CCS heavily depends on the suitability of geologic storage at any given location, however cost considerations are evolving rapidly. For example, it is unclear whether potential for conventional porous media storage of supercritical CO_2 is even possible in certain areas in the US, or how far apart two neighboring CCS projects are required to be to prevent overpressure and mitigate risks.

This thesis study aimed to understand the suitability of CCS for large-scale deployment by 1) exploring and identifying areas where CO_2 storage is or is not possible, 2) providing CO_2 storage costs ($ USD/ton CO_2) utilizing a new cost methodology that considers estimated storage area and injectivity calculations, and 3) providing a geodatabase with said findings for public use.

As a result, the sedimentary CO_2 storage window was used to identify areas of potential CO_2 storage to assess the suitability of CCS for large-scale deployment. This newly created nationwide storage window provides a coherent database that re-evaluates the storage feasibility in sedimentary rocks utilizing national spatial data. The results show storage low to low-medium potential in states like New Mexico, Kansas, and Nebraska, while most of the western states and a large portion of Alaska show areas of no storage

potential. Although the new potential areas have generally lower storage potential compared to other more favorable areas, the lower potential areas can act as a smaller, more localized, and potentially cheaper CO_2 storage alternative. Depending on the distance, number of emissions that need to be transported, and/or the capture technology in place, it is possible that storing CO_2 in closer, less traditional sinks is cheaper than building the infrastructure to transport the fluid.

Additionally, a CO_2 storage cost spatial distribution database was created to assess the suitability of CCS for large-scale deployment. The CO_2 storage costs were calculated using a new cost methodology based on pressure-based capacity and injectivity calculations. Pressure-based capacity is a key concept since it can determine the extent of a project (area per project) based on how much capacity is needed at a certain location. For this analysis, the storage cost spatial distribution depends on a constant total capacity of 20 Mt per project, with a 1 Mtpa injection rate goal for 20 years. With these assumptions, the CO_2 storage cost results show a distribution ranging from \$4.7 to \$51.7 per ton CO_2, varying per location. For areas with potential storage (as indicated by the storage window data) but do not have enough geologic data to calculate capacity nor injectivity, storage costs are estimated utilizing the high percentile results (P90) from the CO_2 storage cost spatial distribution database. Storage costs for these areas are estimated to cost over \$52.4 per ton of CO_2.

Finally, the storage window and storage cost data calculated in this thesis are amalgamated as the *"CO_2 Capacity, Injectivity, and Cost*" database. This database contains both the input data from the USGS and GCCC databases, as well as the output data from this thesis study's analyses.

There are considerable limitations to both the data and analysis utilized in this study. Such limitations include data limitations such as poorly constrained average values

and simplified average values; geologic limitations which include induced seismicity risks and fault compartmentalization; and results limitations, which are based on the decisions made when processing the input data. However, the results and database presented here are promising, and provide the foundation and methodology needed for a more refined version of this work.

9.2 FUTURE WORK

Future work can focus on database improvement by incorporating more detailed, high resolution input spatial data from other national databases. Similar to the data presented in the USGS and GCCC CO_2 databases, the U.S. Department of Energy National Energy Technology Laboratory released their own national carbon atlas storage database (NATCARB, 2015). The NATCARB database contains gridded input data (i.e., porosity, permeability, etc.) for different reservoirs suitable for CO_2 storage across the U.S. Although the NATCARB database was initially considered for this analysis, both unresolved complications in combining the NATCARB data with the GCCC and USGS datasets, as well as a lack of time to resolve such complications prevented NATCARB's incorporation.

Further database improvement efforts include incorporating the data and geologic limitations as discussed in section 8.4.1 and 8.4.2, respectively. For example, the inclusion of geologic limitations such as seismicity and faulting will improve the accuracy of the results, considering seismicity risks would most likely increase the storage prices in the West Coast as it is likely to decrease the maximum acceptable injection pressure and therefore require more wells at wider spacing.

9.2.1 CO_2 Storage Window Improvements

The top and bottom sedimentary CO_2 Storage Window boundaries could be potentially improved with further research efforts. The storage window could be narrowed down by assigning the top boundary window as depth to the bottom of the underground source of drinking water (USDW). The current top window boundary does not consider whether there is deep freshwater at a particular location, which could pose a problem to the development of a potential CCS project. However, data for depth to top of USDW at a nationwide scale is not readily available. Most data encountered are limited to studies performed on one or two regional aquifers, usually within state boundaries (e.g., Hamlin and de la Rocha, 2015, Young et al. 2016). The most promising study for a U.S.-wide depth to top of USDW is (Stanton et al. 2017), but unfortunately only their input data and not their modeled USDW data are publicly available Thus, delineating depth to top of USDW has not been pursued within the contents of this work. Beside the onshore Gulf of Mexico Basin, other U.S. basins have overpressure data (Anadarko: Figure 5 in Nelson and Gianoutsos, 2014). However, the overpressure data is not digitized, and there was not enough time to incorporate this data to the work presented here.

The current version of the CO_2 storage window focuses only on sedimentary rock section of the onshore U.S., but the extent could be further improved if igneous rock (i.e., basalt) were considered for storage potential. Basalt could be a viable, preferred choice in volcanic provinces across the U.S. (e.g., Hawai'i or the Pacific Northwest) at a comparable storage cost to sedimentary reservoirs ($20 - $30 per ton of CO_2, Kelemen et al. 2018) Similarly, offshore storage along the Atlantic Coast (Goldberg et al. 2010) could be considered. Some basalts, such as the Columbia River Basalt Group in Washington State, have been thoroughly researched and have good data to calculate storage (Burns et al.

2011). CO_2 storage in basalts has its own caveats but will not be further discussed in this thesis.

Appendix A

Basin	System	Total Project Costs ($ MM USD)	Storage Costs ($ USD per ton CO2)
Alaska North Slope	Carboniferous	124.38	6.22
Alaska North Slope	Cretaceous	128.68	6.43
Anadarko and Southern Oklahoma Basins	Devonian	1000.24	50.01
Anadarko and Southern Oklahoma Basins	Mississippian	232.3	11.62
Anadarko and Southern Oklahoma Basins	Permian	295.37	14.77
Appalachian Basin	Lower Silurian	405.65	20.28
Appalachian Basin	Ordovician-Cambrian	576.06	28.8
Appalachian Basin	Upper Silurian	694.27	34.71
Arkoma Basin	Carboniferous	2232.04	111.6
Arkoma Basin	Ordovician	118.45	5.92
Arkoma Basin	Silurian - Devonian	1270.17	63.51
Bend Arch and Fort Worth Basin	Fort Worth Basin Carboniferous	220.01	11
Bend Arch and Fort Worth Basin	Fort Worth Basin Ordovician - Mississippian	531.25	26.56
Bighorn Basin	Cretaceous	110.34	5.52
Bighorn Basin	Pennsylvanian	208.52	10.43
Bighorn Basin	Permian	928.59	46.43
Bighorn Basin	Triassic	913.18	45.66
Eastern Great Basin	Jurassic	473.33	23.67
Eastern Mesozoic Rift Basin	Triassic	461.23	23.06
Greater Green River Basin	Cretaceous	876.44	43.82
Greater Green River Basin	Paleozoic	668.04	33.4
Greater Green River Basin	Triassic-Jurassic	229.15	11.46
Hanna, Laramie, and Shirley Basins	Cretaceous	142.83	7.14
Hanna, Laramie, and Shirley Basins	Paleozoic	99.58	4.98
Illinois Basin	Cambrian	131.49	6.57
Illinois Basin	Devonian-Silurian	192.81	9.64
Kandik Basin	Devonian	468.19	23.41
Kandik Basin	Permian	489.82	24.49
Kansas Basins	Paleozoic	316.89	15.84

Basin	System	Total Project Costs ($ MM USD)	Storage Costs ($ USD per ton CO2)
Michigan Basin	Devonian	729.43	36.47
Michigan Basin	Ordovician-Cambrian	137.23	6.86
Michigan Basin	Silurian	184.92	9.25
Palo Duro Basin	Permian	140.68	7.03
Paradox Basin	Paleozoic	512.67	25.63
Permian Basin	Paleozoic	92.43	4.62
Powder River Basin	Jurassic	861.01	43.05
Powder River Basin	Pennsylvanian	168.54	8.43
Powder River Basin	Triassic	1131.24	56.56
Sacramento Basin	Cretaceous	83.39	4.17
Sacramento Basin	Eocene	188.04	9.4
San Joaquin Basin	Cretaceous	83.36	4.17
San Joaquin Basin	Miocene	81.46	4.07
San Joaquin Basin	Oligocene	84.83	4.24
San Juan Basin	Cretaceous	181.64	9.08
U.S. Gulf Coast	Jurassic	99.5	4.98
U.S. Gulf Coast	Miocene	79.09	3.95
Uinta and Piceance Basin	Cretaceous	853.07	42.65
Uinta and Piceance Basin	Paleozoic	449.79	22.49
Uinta and Piceance Basin	Tertiary	453.2	22.66
Ventura Basin	Oligocene	87.22	4.36
Western Oregon-Washington Basins	Washington Basins Paleogene	84.56	4.23
Williston Basin	Cambrian and Ordovician	151.37	7.57
Williston Basin	Cretaceous	235.56	11.78
Williston Basin	Devonian	108.66	5.43
Williston Basin	Jurassic	259.76	12.99
Wyoming-Idaho-Utah Thrust Belt	Cretaceous	463.9	23.19
Wyoming-Idaho-Utah Thrust Belt	Paleozoic	321.11	16.06
Wyoming-Idaho-Utah Thrust Belt	Triassic-Jurassic	112.64	5.63

Table A1: Storage and CCS project costs for all Systems throughout the U.S, single-value results.

Basin	System	Total Project Costs ($ MM USD)						Storage Costs ($ USD per ton CO2)					
		mean	min	P10	P50	P90	max	mean	min	P10	P50	P90	max
Anadarko and Southern Oklahoma Basins	Cambrian	502.39	451.80	456.24	463.00	530.87	728.72	25.12	22.59	22.81	23.15	26.54	36.44
Appalachian Basin	Devonian	1077.67	216.45	439.13	749.88	1332.18	4999.54	53.88	10.82	21.96	37.49	66.61	249.98
Atlantic Coastal	Plain Cretaceous	570.43	83.90	154.29	272.45	809.41	4807.74	28.52	4.19	7.71	13.62	40.47	240.39
Black Warrior	Mississippian	105.17	99.03	100.97	102.37	104.62	344.74	5.26	4.95	5.05	5.12	5.23	17.24
Denver Basin	Cretaceous	123.76	110.60	116.48	120.13	126.91	168.89	6.19	5.53	5.82	6.01	6.35	8.44
Illinois Basin	Ordovician	1063.53	165.38	500.30	704.41	1221.15	4961.32	53.18	8.27	25.01	35.22	61.06	248.07
Los Angeles Basin	Miocene	120.73	84.03	90.91	98.29	117.99	667.81	6.04	4.20	4.55	4.91	5.90	33.39
Michigan basin	Ordovician-Cambrian	271.37	123.65	137.30	184.26	290.35	4537.90	13.57	6.18	6.86	9.21	14.52	226.89
Palo Duro Basin	Paleozoic	111.59	88.23	105.42	109.42	115.79	140.47	5.58	4.41	5.27	5.47	5.79	7.02
Permian Basin	Permian	139.27	115.08	118.97	121.05	126.70	2703.84	6.96	5.75	5.95	6.05	6.33	135.19
Powder River Basin	Cretaceous	131.03	98.06	115.18	133.70	145.37	174.87	6.55	4.90	5.76	6.69	7.27	8.74
San Juan Basin	Jurassic	115.59	106.75	113.16	115.23	117.47	247.95	5.78	5.34	5.66	5.76	5.87	12.40
South Florida Basin	Cretaceous	154.44	110.80	137.29	147.12	166.48	216.88	7.72	5.54	6.86	7.36	8.32	10.84
U.S. Gulf Coast	Cretaceous	305.88	88.21	147.07	193.57	405.27	2856.31	15.29	4.41	7.35	9.68	20.26	142.82
U.S. Gulf Coast	Eocene	125.75	82.52	88.20	94.23	105.71	4268.77	6.29	4.13	4.41	4.71	5.29	213.44
U.S. Gulf Coast	Oligocene	114.81	83.09	88.41	93.03	105.59	4193.56	5.74	4.15	4.42	4.65	5.28	209.68
Williston Basin	Carboniferous	147.32	119.64	133.75	144.71	156.09	258.45	7.37	5.98	6.69	7.24	7.80	12.92

Table A2: Storage and CCS project costs for all Systems throughout the U.S, multiple value (gridded data) results

References

Abba, M.K, Abbas, A.J, Nsr, G.G, Al-Otaibi, A., Burby, M., Saidu, B., and Suleiman, M., 2019, Solubility trapping as a potential secondary mechanism for CO2 sequestration during enhanced gas recovery by CO2 injection in conventional natural gas reservoirs: An experimental approach, Journal of Natural Gas Science and Engineering, v. 71, 103002, https://doi.org/10.1016/j.jngse.2019.103002

Adams, R. L, 1997, Microbasin Analysis of South Louisiana: An Exploration Model, or Hutton and Lyell Were Wrong! Transactions of the Gulf Coast Association of Geological Societies; 47: 1-12.

Anderson, S.T., and Jahediesfanjani, H., 2020, Estimating the net costs of brine production and disposal to expand pressure-limited dynamic capacity for basin-scale CO2 storage in a saline formation, International Journal of Greenhouse Gas Control, v.102, 103161, ISSN 1750-5836, https://doi.org/10.1016/j.ijggc.2020.103161

Baik, E., Sanchez, D.L., Turner, P.A., Mach, K.J., Field, C.B., and Benson, S., 2018, Geospatial analysis of near-term potential for carbon-negative bioenergy in the United States, PNAS, v. 115, no. 13, p. 3290-3295, https://doi.org/10.1073/pnas.1720338115

Bennett, J.A., Ogland-Hand, J.D., Cox, K.J., Johnson, P.J., Middleton, E.J., Pompilio, A.I., Samal, S., Talsma, C.J., Vesselinov, V.V., Ellet, K.M., Middleton, R.S., 2022, Beam Me Up SCO2TPRO: A Comparison to the FE/NETL CO2 Saline Storage Cost Model and Updates on Tool Development, Proceedings of the 16th Greenhouse Gas Control Technologies Conference (GHGT-16) 23-24 Oct 2022, http://dx.doi.org/10.2139/ssrn.4275200

Blackwell, D.D., and M. Richards, 2004, Geothermal Map of North America, AAPG Map, scale 1:6,500,000, Product Code 423, 2004

Bump, A.P., Hovorka, S.D., and Meckel, T.A., 2021, Common risk segment mapping: Streamlining exploration for carbon storage sites, with application to coastal Texas and Louisiana, International Journal of Greenhouse Gas Control, V.11, ISSN 1750-583, https://doi.org/10.1016/j.ijggc.2021.103457

Burke, L.A., Kinney, S.A., Dubiel, R.A., and Pitman, Janet, 2012, Regional map of the 0.70 psi/ft pressure gradient and development of the regional geopressure- gradient model of onshore and offshore Gulf of Mexico, GCAGS

Burns, E.R., Morgan, D.S., Peavler, R.S., and Kahle, S.C., 2011, Three-dimensional model of the geologic framework for the Columbia Plateau Regional Aquifer System, Idaho, Oregon, and Washington: U.S. Geological Survey Scientific Investigations Report 2010-5246, 44 p., http://pubs.usgs.gov/sir/2010/5246

Carbon Solutions LLC, 2022, SCO2TPRO, accessed April 7th 2023 at https://www.carbonsolutionsllc.com/software/sco2t/

Compagnie Generale de Geophysique (CGG), 2019, CGG Robertson Sedimentary Basins of the World - shapefile, Robertson Basins & Play, download data at: https://www.arcgis.com/home/item.html?id=9845f1f30a1641efbe54dd1f9c8c668b

Coleman, J.L., Jr., and Cahan, S.M., 2012, Preliminary catalog of the sedimentary basins of the United States: U.S. Geological Survey Open-File Report 2012–1111, 27 p. (plus 4 figures and 1 table available as separate files) Available online at http://pubs.usgs.gov/of/2012/1111/

De Graaf, I.E.,M.,Rens L.P.H. van Beek, Tom Gleeson, Nils Moosdorf, Oliver Schmitz, Edwin H. Sutanudjaja, Marc F.P. Bierkens, A global-scale two-layer transient groundwater model: Development and application to groundwater depletion, Advances in Water Resources, Volume 102, 2017, Pages 53-67, ISSN 0309-1708, https://doi.org/10.1016/j.advwatres.2017.01.011.

Eaton, B.A., and Eaton, L.E., 1997, Fracture Gradient Prediction for the New Generation, World Oil, vol. 218 (10), 93 p, ISSN: 0043-8790

Ellet, K.M., Middleton, R.S., Stauffer, P.H., Rupp, J.A., 2017, Facilitating CCS business planning by extending functionality of the SimCCS integrated system model, Energy Procedia, v. 114, p. 6526-6535, https://doi.org/10.1016/j.egypro.2017.03.1788

Elliot, J.R., and Lira, C.T., 2012, Ch 7: Engineering Equations of State for PVT Properties in Introductory Chemical Engineering Thermodynamics (2nd edition), Pearson Education, Inc., 912 p. ISBN-13: 978-0-13-606854

Ellsworth, W.L., 2013, Injection-Induced Earthquakes, Science, v.341, issue 6142, ISSN: 0036-8075, 7 p., https://doi.org/10.1126/science.1225942

EPA, 2010, Geologic CO2 Sequestration Technology and Cost Analysis, 67 p. , https://www.epa.gov/sites/default/files/2015-07/documents/support_uic_co2_technologyandcostanalysis.pdf

Ferguson, G., McIntosh, J.C., Grasby, S.E., Hendry, M.J., Jasechko, S., Linsay, M.B., and Luijendijk, E., 2018, The Persistence of Brines in Sedimentary Basins, Geophysical Research Letters, v. 45 (10), p. 4851-4858, https://doi.org/10.1029/2018GL078409

Fick, S.E., and Hijmans, R.J, 2017, WorldClim 2: new 1km spatial resolution climate surfaces for global land areas, International Journal of Climatology, v. 37 (12), pg. 4302-4315, https://doi.org/10.1002/joc.5086

Fish, J.R., and Wood, T.R., 2008, Geologic Carbon Sequestration, Property Rights and Regulation, 54 Rocky Mtn, Min.L,*supra* note 63, 3-16.

Frailey, S.M., Tucker, O., and Koperna, G.J., 2017, The genesis of the CO_2 storage resources management system (SRMS), Energy Procediam v, 114, p. 4262-4269, https://doi.org/10.1016/j.egypro.2017.03.1566

Garrity, C.P., and Soller, D.R., 2009, Database of the Geologic Map of North America; adapted from the map by J.C. Reed, Jr. and others (2005): U.S. Geological Survey Data Series 424 by Roger Palmer for the Esri TESS lessons.

Global CCS Institute, 2019, The Global Status of CCS: Targeting Climate Change, Australia.

Goldberg, D. S., Kent, D. V., and Olsen, P. E, 2010, Potential on-shore and off-shore reservoirs for CO2 sequestration in Central Atlantic magmatic province basalts, Proc. Natl. Acad. Sci. U.S.A. v. 107, p. 1327–1332, https://doi: 10.1073/pnas.0913721107

Gollakota, S., and McDonald, S., 2014, Commercial-scale CCS Project in Decatur, Illinois – Construction Status and Operational Plans for Demonstration, Energy Prodecia, v. 63, p. 5986-5993, https://doi.org/10.1016/j.egypro.2014.11.633

Gulf Coast Carbon Center, 2012, CO2 Brine Database: Sequestration of Greenhouse Gases in Brine Formations, Bureau of Economic Geology, shapefile data available at https://www.beg.utexas.edu/gccc/research/brine-main

Guo, B., Sun, K., Ghalambor, A., 2008, Well Productivity Handbook: Vertical, Fractured, Horizontal, Multilateral, and Intelligent Wells, Gulf Publishing Company, ISBN-10: 1-933762-32-2, 367 p.,

Hamlin, H.S., and de la Rocha, L., 2015, Using Electric Logs to Estimate Groundwater salinity and Map Brackish Groundwater Resources in the Carrizo-Wilcox Aquifer in South Texas, GCAGS Journal, v.4, p. 109-131.

Harrison, F.W., III, 1980, The role of pressure, temperature, salinity, lithology, and structure in hydrocarbon accumulation in Constance Bayou, Deep Lake, and southeast Little Pecan Lake Fields, Cameron Parish, Louisiana: Transactions Gulf Coast Association of Geological Societies, v. 30, p. 113–129, https://doi.org/10.1306/2F91962A-16CE-11D7-8645000102C1865D

Hoffman, N., Carman, G., Bagheri, M, and Goebel, T., 2015, Site Characterization for Carbon Sequestration in the Nearshore Gippsland Basin, SEG Global Meeting Abstracts, p. 265, https://doi.org/10.1190/ice2015-2209980

Hovorka, S. D., 2013, Three-million-metric-ton-monitored injection at the SECARB Cranfield project—project update: Energy Procedia, v. 37, p. 6412–6422, https://doi.org/10.1016/j.egypro.2013.06.571

IEA, 2019 Levelised cost of CO2 capture by sector and initial CO2 concentration, 2019, IEA, Paris https://www.iea.org/data-and-statistics/charts/levelised-cost-of-co2-capture-by-sector-and-initial-co2-concentration-2019

IEA, 2021, Is carbon capture too expensive?, IEA, Paris https://www.iea.org/commentaries/is-carbon-capture-too-expensive

IEA, 2022a, Capacity of large-scale CO2 capture projects, current and planned vs. the Net Zero Scenario, 2020-2030, IEA, Paris, IEA. Licence: CC BY 4.0 https://www.iea.org/data-and-statistics/charts/capacity-of-large-scale-co2-capture-projects-current-and-planned-vs-the-net-zero-scenario-2020-2030

IEA, 2022b, Carbon Capture, Utilisation and Storage, IEA, Paris, License: CC BY 4.0, https://www.iea.org/reports/carbon-capture-utilisation-and-storage-2

IEA, 2022c, Indicative CO2 storage cost curve for the United States, onshore, IEA, Paris, Licence: CC BY 4.0, https://www.iea.org/data-and-statistics/charts/indicative-co2-storage-cost-curve-for-the-united-states-onshore

Intergovernmental Panel on Climate Change (IPCC), 2014, Climate Change 2014: Mitigation of Climate Change, 141 p., ISBN 978-92-9169-142-5, https://www.ipcc.ch/site/assets/uploads/2018/03/WGIIIAR5_SPM_TS_Volume-3.pdf

International Energy Agency, 2022, Direct Air Capture: tracking report, IEA, September 2022, Paris https://www.iea.org/reports/direct-air-capture

Ivory-Moore, R., 2022, Pore Space Rights – U.S. Overview, Global CCS Institute, 4 p., https://www.globalccsinstitute.com/wp-content/uploads/2022/05/Brief-Pore-Space-Rights-5.24-12.pdf

Jahediesfanjani, H., Warwick, P.D., and Anderson, S.T., 2018, Estimating the pressure-limited CO2 injection and storage capacity of the United States saline formations: Effect of the presence of hydrocarbon reservoirs, International Journal of Greenhouse Gas Control, v. 79, pg. 14-24, https://doi.org/10.1016/j.ijggc.2018.09.011

Kaven, J. O., Hickman, S. H., McGarr, A. F., and Ellsworth, W. L., 2015, Surface monitoring of microseismicity at the Decatur, Illinois, CO2 sequestration demonstration site, Seismol. Res. Lett., 86, 1096–1101, https://doi.org/10.1785/0220150062

Kelemen, P., Benson, S.M., Pilorgé, H., Psarras, P., and Wilcox, J., 2019, An Overview of the Status and Challenges of CO2 Storage in Minerals and Geological Formations, Frontiers in Climate, v.1, https://doi.org/10.3389/fclim.2019.00009

Labor Energy Partnership, “Building to Net-Zero: A U.S. Policy Blueprint for Gigaton-Scale CO² Transport and Storage Infrastructure,” June 2021, https://laborenergy.org/reports/blueprints/building-to-net-zero/

Laske, G. and Masters, G., 1997, A Global Digital Map of Sediment Thickness, EOS Trans. AGU, 78, F483.

Lu, K., Kordi, M., Hovorka, S.D., Meckel, T.A., and Christopher, C.A., 2013, Reservoir characterization and complications for trapping mechanisms at Cranfield CO2

injection site, International Journal of Greenhouse Gas Control, v. 18, p. 361-374, https://doi.org/10.1016/j.ijggc.2012.10.007

Marshak, S., Stefanie Domrois, Curtis Abert, Timothy Larson, Gary Pavlis, Michael Hamburger, Xiaotao Yang, Hersh Gilbert, and Chen Chen, 2017, The basement revealed: Tectonic insight from a digital elevation model of the Great Unconformity, USA, cratonic platform: Geology, doi:10.1130/G38875.1. GSA Data Repository 2017115.

Mathias, S.A., Hardisty, P.E., Trudell, M.R., and Zimmerman, R.W., 2009, Screening and selection of sites for CO2 sequestration based on pressure buildup, International Journal of Greenhouse Gas Control, Vol. 3 (5), p. 577-585, https://doi.org/10.1016/j.ijggc.2009.05.002

McCoy, S.T, and Rubin, E.S., 2005, Models of CO2 Transport and Storage Costs and Their Importance in CCS Cost Estimates, Fourth Annual Conference on Carbon Capture and Sequestration DOE/NETL, May 2-5th.

Middleton, R.S., Chen, B., Harp, D.R., Kammer, R.M., Ogland-Hand, J.D., Bielicki, J.M., Clarens, A.F., Currier, R.P., Ellet, K.M., Hoover, B.A., McFarlane, D.N., Pawar, R.J., Stauffer, P.H., Viswanathan H.S., and Yaw, S.P., 2020a, Great SCO2T! Rapid tool for carbon sequestration science, engineering, and economics, Applied Computing and Geosciences, v.7, 100035, ISSN 2590-1974, https://doi.org/10.1016/j.acags.2020.100035.

Middleton, R.S., Yaw, S.P., Hoover, B.A., and Ellet, K.M., 2020b, SimCCS: An open-source tool for optimizing CO2 capture, transport, and storage infrastructure, Environmental Modelling & Software, v.124, 104560, ISSN 1364-8152, https://doi.org/10.1016/j.envsoft.2019.104560

Middleton, R.S., Bennett, J., Ellett, K., Ford, M., Johnson, P. ,Middleton, E., Ogland-Hand, J., and Talsma, C., 2022, Reaching Zero: Pathways to Decarbonize the US Electricity System with CCS, Proceedings of the 16th Greenhouse Gas Control Technologies Conference (GHGT-16), 23-24 Oct 2022, http://dx.doi.org/10.2139/ssrn.4274085

Morrow, C.A., Kaven, J.O., Moore, D.E., and Lockner, D.A., 2017, Physical properties of sidewall cores from Decatur, Illinois: U.S. Geological Survey Open-File Report 2017–1094, 21 p., https://doi.org/10.3133/ofr20171094.

National Petroleum Council, 2021, Meeting the Dual Challenge: A roadmap to At-Scale Deployment of Carbon Capture, Use, and Storage, Vol III Ch. 7, 38 p. ISBN: 979-8705336814, https://dualchallenge.npc.org/downloads.php

Nehring Associates Inc., 2012, The significant oil and gas fields of the United States database, Colorado Springs, Colo., Nehring Associates, Inc., database available from Nehring Associates, Inc., P.O. Box 1655, Colorado Springs, CO 80901, U.S.A.

Nelson, P.H. and Gianoutsos, N.J., 2014, Present-day overpressure and paleopressure indicators in the greater Anadarko Basin, Oklahoma, Texas, Kansas, and Colorado, chap. 8, in Higley, D.K., comp., Petroleum systems and assessment of undiscovered oil and gas in the Anadarko Basin Province, Colorado, Kansas, Oklahoma, and Texas— USGS Province 58: U.S. Geological Survey Digital Data Series DDS–69–EE, 28 p., http://dx.doi.org/10.3133/ds69EE.

National Energy Technology Laboratory (NETL), 2013, Summary of Costs Associated with Seismic Data Acquisition and Processing worksheet, FE/NETL CO2 Saline Storage Cost Model, DOE/NETL-2014/1671.

National Energy Technology Laboratory (NETL), 2015, National Carbon Sequestration Database and Geographic Information System (NATCARB), U.S. Department of Energy, https://www.netl.doe.gov/coal/carbon-storage/strategic-program-support/natcarb-atlas

National Energy Technology Laboratory (NETL), 2017, FE/NETL CO2 Saline Storage Cost Model, U.S. Department of Energy, Last Update: Sep 2017 (Version 3) https://www.netl.doe.gov/research/energy-analysis/search-publications/vuedetails?id=2403

Pett-Ridge, Jennifer, Mark Ashton, Sarah E. Baker, Bruno Basso, Mark Bradford, Hanna Breunig, Alex Bump, Ingrid Busch, Edna Rodriguez Calzado, Jackson W. Chirigotis, Mark Ducey, Jerome Dumortier, Nathan C. Ellebracht, Ramon Gil Egui, Ames Fowler, Katerina Georgiou, Hannah Goldstein, Dermot Hayes, Chad Hellwinckel, Susan Hovorka, Elwin Hunter-Sellars, Whitney Kirkendall, Sara Kuebbing, Patrick Lamers, Matthew Langholtz, Mark Layer, Reid Lewis, Wenqin Li, Allegra Mayer, Kimberley K. Mayfield, Peter Nico, Simon H. Pang, Keith Paustian, George Peridas, Helene Pilorge, Sasha Ponomareva, Lydia Price, Peter Psarras, Phil Robertson, Joe W. Sagues, Daniel Sanchez, Corinne Scown, Briana M. Schmidt, Eric W. Slessarev, Alexander J. Stanley, Amy Swan, Crystal Toureene, Andrew A. Wong, Ethan Woods, Mark Mba Wright, Yao Zhang, Roger D. Aines, Initial Considerations for Large-Scale Carbon Removal in the United States: Description of Methods, Feedstocks, and Constraints, March, 2022, Lawrence Livermore National Laboratory, LLNL-TR-832805-DRAFT

Porter, C.; Morin, P., Howat, I., Noh, M-J, Bates, Brian; Peterman, Kenneth; Keesey, Scott; Schlenk, Matthew; Gardiner, Judith; Tomko, Karen; Willis, Michael; Kelleher, Cole; Cloutier, Michael; Husby, Eric; Foga, Steven; Nakamura, Hitomi; Platson, Melisa; Wethington, Michael, Jr.; Williamson, Cathleen; Bauer, Gregory; Enos, Jeremy; Arnold, Galen; Kramer, William; Becker, Peter; Doshi, Abhijit; D'Souza, Cristelle; Cummens, Pat; Laurier, Fabien; Bojesen, Mikkel, 2018, "ArcticDEM", Harvard Dataverse, V1, September 15th 2022, https://doi.org/10.7910/DVN/OHHUKH

Robinson, D.B., and Peng, D.Y., 1976, A New Two-Constant Equation of State Industrial and Engineering Chemistry: Fundamentals. Industrial & Engineering Chemistry Fundamentals, 15, 59-64, http://dx.doi.org/10.1021/i160057a011

Shah, A.K, and Boyd, O.S., 2018, Depth to basement and thickness of unconsolidated sediments for the western United States—Initial estimates for layers of the U.S. Geological Survey National Crustal Model: U.S. Geological Survey Open-File Report 2018–1115, 13 p., https://doi.org/10.3133/ofr20181115

Smith, E.E, 2021, The cost of CO2 transport and storage in global integrated assessment modeling. MS Thesis, MIT Institute for Data, Systems and Society, http://globalchange.mit.edu/publication/17661

Stanton, J.S., Anning, D.W., Brown, C.J., Moore, R.B., McGuire, V.L., Qi, S.L., Harris, A.C., Dennehy, K.F., McMahon, P.B., Degnan, J.R., and Böhlke, J.K., 2017, Brackish groundwater in the United States: U.S. Geological Survey Professional Paper 1833, 185 p., https://doi.org/10.3133/pp1833

Schruben, P.G., Arndt, R.E., and Bawiec, W.J., 1997, Geology of the Conterminous United States at 1:2,500,000 Scale--A Digital Representation of the 1974 P.B. King and H.M. Beikman Map, U.S. Geological Survey.

SLB Energy Glossary, 2023, Poisson's Ratio, accessed February 1st, 2023, https://glossary.slb.com/en/terms/p/poissons_ratio

Sokolnikoff, I.S.,1983, Mathematical theory of elasticity (2nd ed. reprint), Krieger Publishing Company, 476 p.

S.986 - 117th Congress (2021-2022): Carbon Capture, Utilization, and Storage Tax Credit Amendments Act of 2021. Congress.gov, Library of Congress, 25 March 2021, https://www.congress.gov/bill/117th-congress/senate-bill/986.

Tiab, D., and Donaldson, E.C., 2016, Chapter 2: Introduction to Petroleum Geology, Petrophysics (4th Edition), Gulf Professional Publishing, p. 23-66, https://doi.org/10.1016/B978-0-12-803188-9.00002-4.

Thomas, W.A., 1993 Low-angle detachment geometry of the late Precambrian- Cambrian Appalachian-Ouachita rifted margin of southeastern North America, Geology, v. 24, p. 921-924, https://doi.org/10.1130/0091-7613(1993)021<0921:LADGOT>2.3.CO;2

U.S. Department of State, 2021, The Long-Term Strategy of the United States: Pathways to Net-Zero Greenhouse Gas Emissions by 2050. November2021, United States Department of State, United States Executive Office of the President: Washington DC. https://www.whitehouse.gov/wp-content/uploads/2021/10/US-Long-Term-Strategy.pdf

U.S. Energy Information Administration (EIA), 2011, U.S. Sedimentary Basins database, last updated 2020, https://atlas.eia.gov/datasets/eia::sedimentary-basins/about

U.S. Geological Survey, 2022, 3D Elevation program (3DEP) Bare Earth DEM Dynamic Service, ArcGIS Online Services, medatadata available at https://elevation.nationalmap.gov/arcgis/rest/services/3DEPElevation/ImageServer

U.S. Geological Survey, 2018, 2018 Short-term Induced Seismicity Models, Earthquake Hazards Program, https://www.usgs.gov/media/images/short-term-seismicity-model-2018

U.S. Geological Survey Geologic Carbon Dioxide Storage Resources Assessment Team, 2013, National assessment of geologic carbon dioxide storage resources—Data (ver. 1.1, September 2013): U.S. Geological Survey Data Series 774, 13 p., plus 2 appendixes and 2 large tables in separate files, https://pubs.usgs.gov/ds/774/. (Supersedes ver. 1.0 released June 26, 2013.)

Van der Meer, L.G.H, and Yavuz, F., 2009, CO2 storage capacity calculations for the Dutch subsurface, GHGT-9, Energy Procedia, v. 1, p. 2615-2622, https://doi.org/10.1016/j.egypro.2009.02.028

Valluri, M., Mishra, S., Ganesh, P.R., 2020, Injectivity index: a powerful tool for characterizing CO2 storage reservoirs—a technical note, Greenhouse Gases science and Technology, v. 11, i. 2, p. 251-265, https://doi.org/10.1002/ghg.2046

Verdon, J.P., Kendall, J.M., Stork, A.L., Chadwick, R.A., White, D.J., and Bissel. R.C., 2013, Comparison of geomechanical deformation induced by megatonne-scale CO2 storage at Sleipner, Weyburn, and In Salah, Pro National Academy of Science, v. 110, i. 30, p. E2762-71, https://www.pnas.org/doi/pdf/10.1073/pnas.1302156110

Vilarrasa, V., Carrera, J., Olivella, S., Rutqvist, J., and Laloui, L., 2019, Induced Seismicity in Geologic Carbon Storage, Solid Earth Open Access, 10, 871–892, https://doi.org/10.5194/se-10-871-2019

Wallace, K.J., Meckel, T.A., Carr, D.L., Treviño, R.H., and Yang, C., 2014, Regional CO2 sequestration capacity assessment for the coastal and offshore Texas Miocene interval. Greenhouse Gases: Science and Technology, 4(1), 53-65. http://dx.doi.org/10.1002/ghg.1380

Wilson, F.H., Hults, C.P., Mull, C.G, and Karl, S.M, compilers, 2015, Geologic map of Alaska: U.S. Geological Survey Scientific Investigations Map 3340, pamphlet 196 p., 2 sheets, scale 1:1,584,000, https://doi.org/10.3133/sim3340.

Young, S.C., Jigmond, M., Deeds, N., Blainey, J., Ewing, and Banerj, D., 2016, Identification of Potential Brackish Groundwater Production Areas – Gulf Coast Aquifer System, INTERA, Inc., TWDB contract number: 1600011947, https://www.twdb.texas.gov/groundwater/bracs/projects/HB30_Gulf_Coast/index.asp

Zadick, J.R., 2011, The Public Pore Space: Enabling Carbon Capture and Sequestration by Reconceptualizing Subsurface Property Rights, 36 Wm. and Mary Envtl. L. & Pol'y Rev. 257, https://scholarship.law.wm.edu/wmelpr/vol36/iss1/9